Fuel 220 (2018) 725–743

Contents lists available at ScienceDirect

Fuel

journal homepage: www.elsevier.com/locate/fuel

Full Length Article

Integration of chemical looping oxygen production and chemical looping combustion in integrated gasification combined cycles

Schalk Cloete[a], Antonio Giuffrida[b], Matteo Romano[b], Paolo Chiesa[b], Mehdi Pishahang[a], Yngve Larring[a,*]

[a] SINTEF Materials and Chemistry, Trondheim, Norway
[b] Department of Energy, Politecnico di Milano, Milan, Italy

ARTICLE INFO

Keywords:
Chemical looping oxygen production
Chemical looping combustion
COMPOSITE
Integrated gasification combined cycle
CO_2 capture
Energy penalty

ABSTRACT

Energy penalty is the primary economic challenge facing CO_2 capture technology. This work aims to address this challenge through a novel power plant configuration, capable of achieving 45.4% electric efficiency from coal with a 95% CO_2 capture efficiency. The COMPOSITE concept integrates chemical looping oxygen production (CLOP) and packed bed chemical looping combustion (PBCLC) reactors into an integrated gasification combined cycle (IGCC) power plant. Hot gas clean-up technology is implemented to boost plant efficiency. When commercially available cold gas clean-up technology is used, the plant efficiency reduces by 2%-points, but remains 2.3%-points higher than a comparative PBCLC-IGCC power plant and 8.1%-points higher than an IGCC power plant with pre-combustion CO_2 capture. It was also shown that the COMPOSITE power plant performance was not sensitive to changes in the performance of the CLOP reactors, implying that uncertainties related to this novel process component do not reduce the potential of the COMPOSITE concept. The outstanding efficiency obtained for this concept is made possible by a complex and highly integrated plant configuration, whose operability and techno-economic feasibility must be demonstrated.

1. Introduction

Energy penalty is the primary economic challenge facing CO_2 capture processes. The energy requirements of CO_2 capture not only increase fuel consumption, but also increase plant capital costs (a larger plant is required to produce a given amount of power) as well as the amount of CO_2 that needs to be captured, transported and stored. According to a recent review of the costs of CCS [1], a typical pulverized coal (PC) plant with post-combustion CO_2 capture will require about 32% more energy per unit electricity production than an equivalent plant without CO_2 capture. This is a major contributing factor to the ~62% increase in the levelized cost of electricity.

For this reason, energy efficiency has been the highest CO_2 capture research priority. Several second-generation CO_2 capture processes have been proposed with the primary aim of reducing energy penalty. Chemical looping technologies offer the most fundamental potential for achieving this goal because inherent separation between CO_2 and N_2 is achieved with almost no associated energy cost.

Chemical looping combustion (CLC) [2] is the most studied chemical looping configuration. It operates by transporting oxygen from air to fuel using an oxide oxygen carrier material (OCM). Air and fuel are fed to two separate reactors where the OCM is oxidized by air, transported to the fuel reactor, reduced by the fuel, and then transported back to the air reactor. This way, CLC achieves oxyfuel CO_2 capture without the large energy penalty associated with air separation.

When applied to solid fuels, CLC can be implemented in two distinctly different configurations. Firstly, integrated gasification CLC (iG-CLC) feeds the solid fuel directly into the fuel reactor where it gasifies and reduces the oxygen carrier. A recent study estimated that iG-CLC can capture CO_2 for only €20/ton relative to a coal plant using a circulating fluidized bed (CFB) boiler [3]. The second alternative is integration of conventional gas-fuelled CLC into an IGCC power plant. This CO_2 capture pathway produces a similar cost increase (€23/ton) relative to an unabated IGCC plant [4].

Both these technology pathways have advantages and drawbacks. The iG-CLC pathway can capitalize on know-how from commercial deployment of CFB boilers. Even though CFB boilers are designed primarily for low-rank coal and have only recently been demonstrated at scale in efficient supercritical configurations, this similarity should be beneficial during the iG-CLC scale-up process. The capital costs of a CFB boiler is generally higher than that of a conventional pulverized coal (PC) boiler, but this capital cost drawback can be recovered by not

* Corresponding author at: Sustainable Energy Process Technology Department, SINTEF Materials and Chemistry, Forskningsveien 1, 0373 Oslo, Norway.
E-mail address: yngve.larring@sintef.no (Y. Larring).

https://doi.org/10.1016/j.fuel.2018.02.048
Received 28 April 2017; Received in revised form 21 August 2017; Accepted 8 February 2018
Available online 22 February 2018

List of symbols

Regular symbols

α	Volume fraction
ε	Void fraction
ϕ	Thiele modulus
η	Effectiveness factor
ρ	Density (kg/m^3)
$\vec{v}$	Velocity vector (m/s)
τ	Tortuosity
$\bar{\bar{\tau}}$	Stress tensor (kg/s^{2}m)
ξ	Normalized radius
C	Molar concentration (mol/m^3)
D	Diffusivity (m^2/s)
d	Diameter (m)
$\vec{g}$	Gravity vector (m/s^2)
h	Enthalpy (J/kg)
$\dot{H}$	LHV flow rate (MW)
$\vec{J}$	Diffusive mass flux (kg/m^{2}s)
K	Equilibrium constant
K_{sg}	Interphase exchange coefficient (kg/m^{3}s)
k	Reaction rate constant ((m/s) (mol/m^3)$^{1-n}$)
M	Molecular weight (kg/mol)
$\dot{m}$	Mass transfer rate (kg/m^{3}s)
$\dot{M}$	Molar flow rate (kmol/s)
N	Moles (mol)
n	Reaction order
P	Pressure (bar)
p	Pressure (Pa)
Q	Interphase heat exchange (J/m^{3}s)
$\vec{q}$	Diffusive energy flux (J/m^{2}s)
R	Universal gas constant (8.314 J/mol.K)
R^H	Heterogeneous reaction rate (mol/m^{3}s)
S	Mass source term (kg/m^{3}s)
$S^{\vec{v}}$	Momentum source term (kg/m^{2}s^2)
S^h	Energy source term (J/m^{3}s)
s	Active surface area (fraction)
T	Temperature (K)
V	Volume (m^3)
w	Degree of solids conversion (fraction)
x	Mole fraction
Y	Mass fraction

Subscripts

c	Active core
eff	Effective
eq	Equilibrium
g	Gas
gr	Grain
i	Species index
p	Particle
ox	Oxidation
pq	Interphase exchange
q	Phase index
red	Reduction
s	Solids

Acronyms

ASU	Air separation unit
CGE	Cold gas efficiency
CLC	Chemical Looping Combustion
CLOP	Chemical Looping Oxygen Production
CLOU	Chemical Looping with Oxygen Uncoupling
CGCU	Cold gas clean-up
HGCU	Hot gas clean-up
HHV	Higher heating value
HP	High pressure
HRSG	Heat recovery steam generator
HT	High temperature
HTW	High temperature Winkler
HV	Heating value
IP	Intermediate pressure
IGCC	Integrated Gasification Combined Cycle
LHV	lower heating value
MP	Medium pressure
OCM	Oxygen carrier material
PBCLC	Packed Bed Chemical Looping Combustion
TOT	Turbine outlet temperature

having to include downstream flue gas scrubbers [5]. However, increasingly strict emissions standards may require flue gas treatment even from CFB plants [5].

IGCC plants are more capital-intensive than PC plants and there are only a few operating plants globally. However, the IGCC configuration is inherently capable of higher efficiencies and lower emissions than PC boilers. It therefore remains a relevant prospect for solid fuel combustion in an increasingly carbon-constrained world with strict emissions standards. IGCC also has significant headroom for future cost reductions through hot gas cleanup and advanced gas turbine technology. By the year 2030, the latest version of the International Energy Agency's electricity cost projections [6] gives similar costs for IGCC (60–88 $/MWh) and advanced ultra-supercritical PC (58–82 $/MWh) plants. The IGCC-based process proposed in this paper can become a commercial reality by the year 2030 and beyond when IGCC should be more competitive.

Regarding the CLC units in the two configurations, the primary technical challenges are in-situ gasification in the iG-CLC configuration and pressurized operation in the IGCC configuration. The iG-CLC technology poses challenges related to fuel slip from syngas produced near the top of the fuel reactor, the need for a carbon stripper unit to prevent char from leaking to the air reactor, and the demand for a very cheap oxygen carrier that can have a short active lifetime due to ash exposure or losses with ash removal [7,8]. For IGCC, pressurized operation greatly increases the required solids circulation rate per unit reactor volume and requires special measures to carry the pressure load on all pressurized components. Technical challenges are also presented by the need for high-temperature filtration of fines that can damage the downstream gas turbine.

In this work, the IGCC pathway is studied. The starting point is based on an earlier work with integrated packed bed CLC (PBCLC) for highly efficient CO_2 separation [9,10]. The PBCLC configuration keeps the oxygen carrier in a single reactor where it is alternatively exposed to air and fuel gases. This simple standalone reactor configuration should be simpler to scale up than the conventional dual fluidized bed CLC configuration, especially under pressurized operation. We propose an extension of this PBCLC-IGCC power plant configuration to further boost the already attractive efficiency by replacing the air separation unit (ASU) with a chemical looping oxygen production (CLOP) unit. A more detailed description of this novel process is given in the next section.

1.1. The COMPOSITE process

The CLOP-PBCLC-IGCC process configuration studied in this work, henceforth called COMPOSITE, is illustrated in Fig. 1. In essence, COMPOSITE is an IGCC plant where the ASU is replaced by CLOP reactors and the combustor is replaced by PBCLC reactors. The PBCLC reactors facilitate CO_2 capture with minimal energy penalty, while the CLOP reactors avoid the energy penalty related to cryogenic air separation. Both reactor systems are implemented as packed beds in this work as will be discussed in more detail in the next section.

It is noted that substantial technological uncertainty is introduced by the low level of maturity of the PBCLC and CLOP reactors. However, this thermodynamic assessment aims only to assess whether a process configuration using these concepts can lead to significant efficiency gains. Good thermodynamic performance of the overall COMPOSITE process can then serve as motivation for dedicated scale-up and demonstration work on the PBCLC and CLOP reactors.

Some attractive synergies exist between the main process units in the COMPOSITE process. The O_2-rich sweep gases going from the CLOP units to the gasifier contain a large amount of CO_2 and H_2O, removing the need for steam addition. Syngas produced by the gasifier has a relatively low heating value, but the high content of CO_2 and H_2O removes the need to recycle flue gases to prevent carbon deposition in the PBCLC units which can lead to significant energy penalties [9]. In addition, the heated depleted air stream entering the PBCLC reactors from the CLOP reactors removes the need for a nitrogen recycle stream when the cheap natural mineral, ilmenite, is used as the OCM [11]. This can be achieved because the reactor will be at a sufficiently high temperature to allow for successful OCM reduction following oxidation with this pre-heated stream. Finally, splitting the fuel between the CLOP and PBCLC reactors also reduces the thermochemical stresses on the OCM and can be expected to increase OCM lifetime, similar to the two-stage PBCLC reactor concept [12].

Even though the scope of this study is limited to process design and efficiency assessment, a few qualitative observations about capital costs can also be made here. Relative to the PBCLC-IGCC plant, which promises CO_2 capture for €23/ton relative to an unabated IGCC benchmark [13], three main differences can be observed. Firstly, the COMPOSITE process is more efficient, thus producing more power from the same capital investment. Secondly, the CLOP reactors should have a similar cost as the avoided ASU, thus imposing no net increase in capital costs. Thirdly, the gasifier and gas cleanup stations will need to be larger given the lower heating value of the produced syngas, thus increasing capital costs. It is difficult to say at present whether the positive effect of higher efficiency will outweigh the negative effect of a larger gas throughput, but the COMPOSITE plant should have similar capital costs to the PBCLC-IGCC plant. In this case, the improved efficiency of COMPOSITE should result in better economics due to lower fuel consumption as well as less CO_2 compression, transport and storage.

1.2. Packed bed CLC and CLOP reactors

As illustrated in Fig. 2, both the PBCLC and CLOP processes operate by alternatively exposing an OCM to oxidation with air and reduction with fuel (and a sweep gas in the CLOP case) using a valve at the reactor inlet. A cluster of such dynamically operated reactors can act as a steady state processing unit that will be relatively simple to scale-up and operate under pressurized conditions.

It is clear that the two processes in Fig. 2 operate in a similar manner with the primary difference being the presence of gaseous

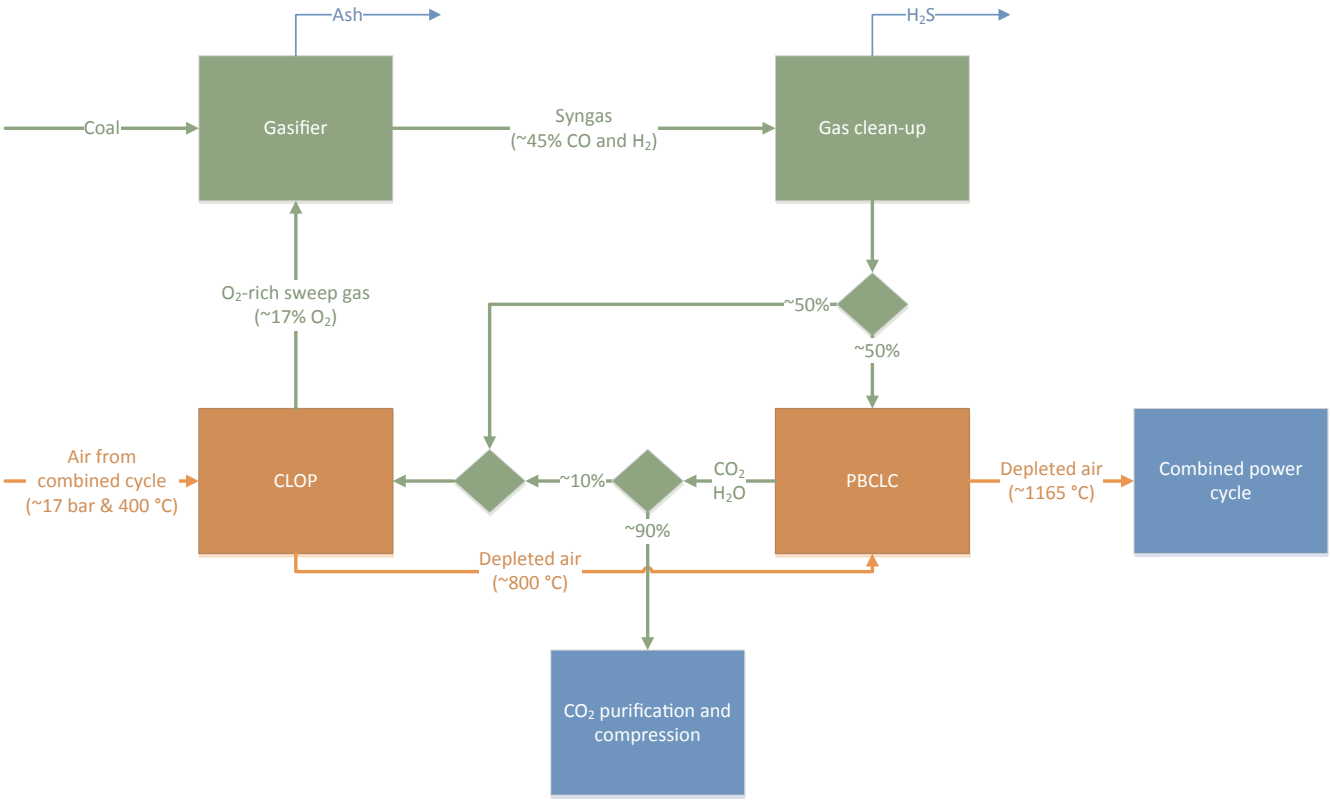

Fig. 1. Schematic diagram of the COMPOSITE process. Green process streams contain carbon, while orange process streams contain nitrogen. Inherent separation of these streams is ensured in the CLOP and PBCLC units (orange). (For interpretation of the references to colour in this figure legend, the reader is referred to the web version of this article.)

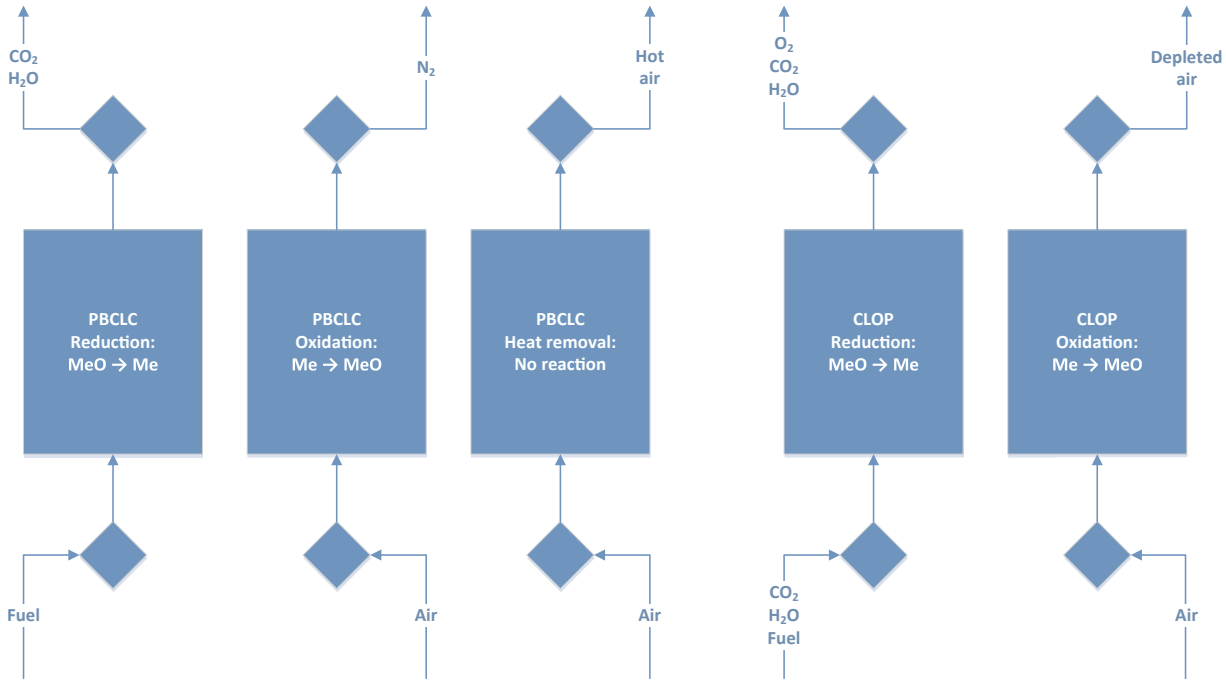

Fig. 2. Schematic of the PBCLC and CLOP reactor operation. Integration of these two reactor concepts into an IGCC power plant is illustrated in Fig. 1.

oxygen in the outlet stream of the CLOP reduction stage. This is achieved by using a CLOU OCM that releases free oxygen under conditions of pressure and temperature that are achievable in an IGCC power cycle. This class of OCMs represents a relatively new field of research, but a number of promising candidates have been identified such as Mn, Co and Cu oxides [14].

The CLOP and PBCLC reactors are the two least mature units in the COMPOSITE process and will be investigated in more detail in this work before the power plant simulations are carried out. Results will therefore be reported in two main sections: reactor simulations of the CLOP and PBCLC reactors and power plant simulations of the COMPOSITE process.

2. Reactor simulations

The two most novel units in the COMPOSITE concept, the CLOP and PBCLC packed bed reactors, will be simulated in more detail using 1D modelling.

2.1. Conservation equations

The continuity equation for each phase (q) is given below where the source term on the right hand side describes interphase mass transfer due to heterogeneous reactions:

$$\frac{\partial}{\partial t}(\alpha_q \rho_q) + \nabla\cdot(\alpha_q \rho_q \vec{v}_q) = \alpha_q S_q \tag{1}$$

Momentum conservation for the gas phase is written as follows with the solids velocity fixed to zero:

$$\frac{\partial}{\partial t}(\alpha_g \rho_g \vec{v}_g) + \nabla\cdot(\alpha_g \rho_g \vec{v}_g \vec{v}_g) = -\alpha_g \nabla p + \nabla\cdot\bar{\bar{\tau}}_g + \alpha_g \rho_g \vec{g} + K_{sg}(\vec{v}_s - \vec{v}_g) + S_g^{\vec{v}} \tag{2}$$

The interphase momentum exchange coefficient (K_{sg}) is described by the Ergun equation [15] and the source term on the far right represents momentum transfer associated with the mass transfer due to heterogeneous reactions.

The energy is conserved for each phase (q) by solving the following enthalpy equation:

$$\frac{\partial}{\partial t}(\alpha_q \rho_q h_q) + \nabla\cdot(\alpha_q \rho_q \vec{v}_q h_q) = -\alpha_q \frac{\partial p_q}{\partial t} + \bar{\bar{\tau}}_q : \nabla\vec{v}_q + \nabla\cdot\vec{q}_q + S_q^h + Q_{pq} + (\dot{m}_{pq} h_{pq} - \dot{m}_{qp} h_{qp}) \tag{3}$$

Heat dispersion in the packed bed (third term on the right) was described via the comprehensive correlation of Tsotsas and Martin [16]. Interphase heat exchange (second last term on the right) is modelled according to Gunn [17].

Furthermore, species conservation equations are solved for each species (i) in each phase (q):

$$\frac{\partial}{\partial t}(\alpha_q \rho_q Y_{qi}) + \nabla\cdot(\alpha_q \rho_q \vec{v}_q Y_{qi}) = \nabla\cdot\alpha_q \vec{J}_{qi} + \alpha_q S_{qi} \tag{4}$$

In the case of the solids phase, the diffusive flux is set to zero.

2.2. Reaction kinetics

The reaction kinetics implemented in this study will be discussed in three parts: CLOP kinetics, PBCLC kinetics and a mass transfer model applied to both reaction systems.

2.2.1. CLOP kinetics

Being a very new application of the chemical looping principle, kinetics for the oxygen uptake and release equilibrium reaction is not yet available for specialized CLOP materials. A preliminary kinetic model was therefore derived from TGA experiments on a $Ca_2AlMnO_{5+\delta}$ material [18] (henceforth abbreviated as CAM) especially for this study. The CAM material reacts according to the following reaction: $\frac{2}{\delta}Ca_2AlMnO_5 + O_2 \leftrightarrow \frac{2}{\delta}Ca_2AlMnO_{5+\delta}$, where $0 < \delta < 0.5$.

Given the novelty of this material, significant uncertainty remains about the kinetics description in this section. This uncertainty is accounted for by making conservative assumptions about the material reactivity and evaluating a range of CLOP reactor performance in the power plant simulations (Section 4.2.2).

Equilibrium behaviour was estimated using the Van't Hoff equation for relating the equilibrium oxygen partial pressure to the temperature with knowledge of the reaction enthalpy. The oxidation enthalpy was estimated as -91 kJ/mol O_2 and a reference temperature of 720 °C at an oxygen partial pressure of 1 bar was determined from TGA studies.

This information allowed for the calculation of the equilibrium oxygen mole fraction at any given temperature and pressure.

$$x_{O_2,eq} = \frac{1}{P}\exp\left(\frac{-91000}{R}\left(\frac{1}{T}-\frac{1}{993.15}\right)\right) \quad (5)$$

The reaction rate was found to have an Arrhenius temperature dependency for reduction (when the local oxygen mole fraction is lower than equilibrium) and no temperature dependency for oxidation (when the local oxygen mole fraction is higher than equilibrium):

$$R_{O_2}^H = -\frac{1}{V}\frac{dN_{O_2}}{dt} = \begin{cases} 7.7\times10^{10}e^{\left(\frac{-174500}{RT}\right)}w_{ox}^{2/3} \ if \ (x_{O_2}-x_{O_2.eq}) \leqslant 0 \\ 27w_{red}^{2/3} \ if \ (x_{O_2}-x_{O_2.eq}) > 0 \end{cases} \quad (6)$$

The degree of OCM conversion, $w_{ox}^{2/3} or w_{red}^{2/3}$, ensures that the reaction rate goes to zero as the OCM becomes completely converted according to the shrinking core model. As shown in Fig. 3, this simplified model produces a reasonable fit with experimental data.

In order to approximate reaction behaviour close to equilibrium conditions, the reaction rate was assumed to increase linearly from zero at equilibrium to a maximum when the actual oxygen mole fraction (x_{O_2}) deviates by 0.1 from the equilibrium oxygen mole fraction ($x_{O_2,eq}$) calculated in Eq. (5). This is a conservative assumption that will significantly reduce the reaction rate relative to the kinetics reported in Eq. (6), thus worsening reactor performance. Adding this component to Eq. (6) yields Eq. (7), which is implemented to describe the oxygen uptake and release in the CLOP simulations.

$$R_{O_2}^H = -\frac{1}{V}\frac{dN_{O_2}}{dt} = \begin{cases} 7.7\times10^{10}e^{\left(\frac{-174500}{RT}\right)}w_{ox}^{2/3}\min(10(x_{O_2}-x_{O_2,eq}),-1) \ if \ (x_{O_2} \\ \quad -x_{O_2.eq}) \leqslant 0 \\ 27w_{red}^{2/3}\max(10(x_{O_2}-x_{O_2,eq}),1) \ if \ (x_{O_2}-x_{O_2.eq}) > 0 \end{cases} \quad (7)$$

Fuel gases (H_2, CO and CH_4) are included in the CLOP reduction stage to increase the overall reactor temperature. These gases must react directly with the OCM at relatively low temperatures for the process to work. At this point, it is unknown whether the CAM material chosen for this study will react directly with the fuel gases. For this reason, a Cu-based OCM is included near the inlet of the reactor. This material is highly reactive even at low temperatures for the following reactions:

$$H_2 + CuO \rightarrow Cu + H_2O$$
$$CO + CuO \rightarrow Cu + CO_2$$
$$CH_4 + 4CuO \rightarrow 4Cu + 2H_2O + CO_2$$
$$O_2 + 2Cu \rightarrow 2CuO$$

It should be noted that this replacement of CAM with CuO will reduce reactor performance because the enthalpy of oxidation of Cu to CuO (−312 kJ/mol O_2) is substantially larger than CAM (−91 kJ/mol O_2). Redox reactions over CuO instead of CAM will therefore release more energy during oxidation where it is desired that the temperature should be low. In other words, if the CAM material can be directly reduced by the fuel gases, most of the heating value of the fuel will be released during reduction, raising the reactor temperature and promoting more release of O_2 according to Eq. (5).

These heterogeneous reactions involving CuO were described by the shrinking core model [19] with chemical kinetics as the rate limiting step on each of the nanoscale grains (0.8 nm in diameter for reduction and 0.52 nm in diameter for oxidation [20]) inside of the particle. The formulation of the volumetric reaction rate of a gaseous reactant is shown below:

$$R_i^H = -\frac{1}{V}\frac{dN_i}{dt} = \frac{6}{d_{gr}}s(1-w)^{2/3}\alpha_s k\left(\frac{Y_i\rho_g}{M_i}\right)^n \quad (8)$$

The active surface area in the particle (s) is 0.1 and the reaction orders (n) for the reactions involving H_2, CO, CH_4 and O_2 are 0.6, 0.8, 0.4 and 1 respectively. The reaction rate constants (k) for different reactions are taken from Abad et al. [20], which found that an increase in pressure reduced the reaction rate constant:

$$k_{H_2} = \frac{1\times10^{-4}}{p^{0.53}}e^{\left(\frac{-33000}{RT}\right)}$$
$$k_{CO} = \frac{5.9\times10^{-6}}{p^{0.83}}e^{\left(\frac{-14000}{RT}\right)}$$
$$k_{CH_4} = 4.5\times10^{-4}e^{\left(\frac{-60000}{RT}\right)}$$
$$k_{O_2} = \frac{4.7\times10^{-6}}{p^{0.68}}e^{\left(\frac{-15000}{RT}\right)} \quad (9)$$

The Cu-based OCM also has the property of oxygen uncoupling, but equilibrium oxygen mole fractions at the high reactor pressures

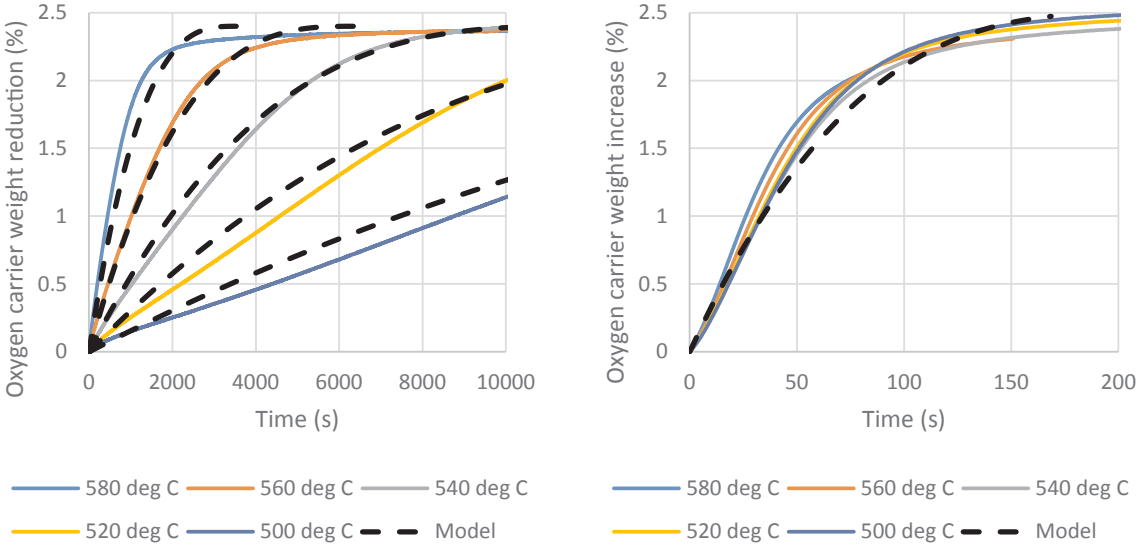

Fig. 3. Comparison between TGA experiments and the kinetic model in Eq. (6) for reduction (left) and oxidation (right). Reduction was carried out in an atmosphere of 100% N_2 and oxidation in an atmosphere of 100% O_2 in order to assess the reaction rates far from equilibrium.

(~15 bar) investigated in this study are very small. Oxygen uncoupling from this material can therefore be safely neglected in this study.

In addition, very fast reactions were specified between all fuel gases and free oxygen to simulate complete combustion of fuel slipping past the Cu-based OCM with oxygen released from the CAM material.

2.2.2. PBCLC kinetics

The PBCLC system uses an ilmenite OCM according to the following simplified heterogeneous reactions:

$$H_2 + Fe_2O_3 \rightarrow 2FeO + H_2O$$
$$CO + Fe_2O_3 \rightarrow 2FeO + CO_2$$
$$CH_4 + 4Fe_2O_3 \rightarrow 8FeO + 2H_2O + CO_2$$
$$O_2 + 4FeO \rightarrow 2Fe_2O_3$$

A similar shrinking core model with chemical kinetics as the rate limiting step on each of the microscopic grains (2.5 μm diameter [21]) was implemented in this case:

$$R_i^H = -\frac{1}{V}\frac{dN_i}{dt} = \frac{6}{d_{gr}}(1-X)^{2/3}\alpha_s k\left(\frac{Y_i\rho_g}{M_i}\right)^n \quad (10)$$

All reaction orders are 1 except for CO, which has a reaction order of 0.8. The reaction rate constants for different reactions are taken from Abad et al. [21]. Similar to the Cu-based kinetics in Eq. (9), the reaction rate constant was assumed to be inversely proportional to the pressure to the power of 0.8. This will result in conservatively slow kinetics being implemented in the model and is based on results from an Fe-based OCM [22].

$$k_{H_2} = \frac{0.062}{p^{0.8}}e^{\left(\frac{-65000}{RT}\right)}$$
$$k_{CO} = \frac{0.1}{p^{0.8}}e^{\left(\frac{-80700}{RT}\right)}$$
$$k_{CH_4} = \frac{9.8}{p^{0.8}}e^{\left(\frac{-135200}{RT}\right)}$$
$$k_{O_2} = \frac{0.0019}{p^{0.8}}e^{\left(\frac{-25500}{RT}\right)} \quad (11)$$

2.2.3. Mass transfer limitation

Substantial mass transfer limitations are also present due to the size of the shaped pellets used in the CLOP and PBCLC reactors. The following intra-particle mass transfer resistance model is implemented to account for this limitation [23].

$$\eta = \frac{3\xi_c^3}{(\xi_c\phi)^2}\frac{\phi\xi_c\coth(\phi\xi_c)-1}{1+(1-\xi_c)(\phi\xi_c\coth(\phi\xi_c)-1)} \quad (12)$$

$$\phi = \frac{d_p}{2}\sqrt{\frac{k_{eff}C^{n-1}}{D_e}} = \frac{d_p}{2}\sqrt{\frac{R^H\left(\alpha_s\frac{Y_i\rho_g}{M_i}\right)^{-1}}{D_e}} \quad (13)$$

$$D_e = \frac{\varepsilon_p D}{\tau} \quad (14)$$

$$\xi_c = \min\left[1, \left(\left(\frac{15}{\phi^2}\right)^{0.6} + (1-w)^{0.4}\right)^{\frac{1}{3}}(1-w)^{0.2}\right] \quad (15)$$

The particle porosity and tortuosity were set to $\varepsilon_s = 0.3$ and $\tau = 2$ respectively. The effectiveness factor ($\eta < 1$) resulting from this model is then multiplied with the reaction rates given in Eq. (7), Eq. (8) and Eq. (10) to model the effect of mass transfer resistance.

2.3. Geometry, materials and boundary conditions

A simple 1D geometry, 10 m in length, was created for both reactors and meshed with 100 cells. This mesh was sufficient to resolve the reaction and heat fronts moving through the packed bed reactor.

The beds were packed with 5 mm particles. The CAM material consisted of three species: $Ca_2AlMnO_{5.5}$ (oxidized), Ca_2AlMnO_5 (reduced) and an inert Ca_2AlMnO_5 which comprised a mass fraction of 0.25 because the TGA results which showed that the oxygen carrying capacity of the material was only 75% of the theoretical maximum. The densities (including the particle porosity) of $Ca_2AlMnO_{5.5}$ and Ca_2AlMnO_5 were 2067 and 2000 kg/m^3 respectively. The Cu-based OCM consisted of CuO (oxidized) with a density of 2799 kg/m^3, Cu (reduced) with a density of 3842 kg/m^3 and an alumina support with a density of 1714 kg/m^3. An active content of 15% was assumed in order to limit the maximum temperature in the material to 950 °C. Lastly, ilmenite was assumed to consist of Fe_2O_3 (oxidized) with a density of 3144 kg/m^3, FeO (reduced) with a density of 2829 kg/m^3 and inert TiO_2 with a density of 2538 kg/m^3. An active content of 19.6% was set to limit the maximum reactor temperature to 1200 °C. The ideal gas law was implemented for calculated gas densities. Heat capacities were implemented as a function of temperature based on the correlations of Robie [24] for the solids and on JANAF thermochemical tables [25] for the gas. The heat capacity of the CAM material was estimated as a summation of heat capacities for its three constituent oxides of CaO, Al_2O_3, and Mn_2O_3, in stoichiometric ratios. The temperature-dependence of these input heat capacity values were extracted from FactSage™ software's database.

Table 1
CLOP reactor inlet streams. As shown in Fig. 1, the reduction stage inlet is combined from a fuel stream from the gas clean up section and a stream of combustion products from the PBCLC unit. The mass flow rates of these streams are adjusted to achieve the desired reactor temperature by changing the parameter x in the table (more fuel leads to a higher reactor temperature), while keeping the total gas flow rate to the reduction stage at 3.54 kg/m^{2}s.

Stream	Stage time (s)	Mass flux (kg/m^{2}s)	Temperature (°C)	Composition (mole fraction)	
Compressed air to oxidation stage	360	5.5	404.4	O_2	0.2073
				H_2O	0.0103
				CO_2	0.0003
				Ar	0.0092
				N_2	0.7729
Fuel to reduction stage	60	3.54 − x	432.2	H_2	0.1184
				CO	0.3549
				CH4	0.0185
				H_2O	0.1584
				CO_2	0.3423
				N_2	0.0075
Combustion products to reduction stage	60	0.04 < x < 0.58	1200	H_2O	0.3026
				CO_2	0.6901
				N_2	0.0073

The PBCLC reactors receive a heated depleted air stream from the CLOP reactors during the oxidation stage and fuel from the gas clean-up unit during the reduction stage. These two streams are specified in Table 2.

Table 2
PBCLC reactor inlet streams.

Stage	Stage time (s)	Mass flux (kg/m^{2}s)	Temperature (°C)	Composition (mole fraction)	
Oxidation	1500	4.2–5.0	800	O_2	0.1642
				H_2O	0.0109
				CO_2	0.0003
				Ar	0.0097
				N_2	0.8149
Reduction	300	2.55	432.2	H_2	0.1184
				CO	0.3549
				CH4	0.0185
				H_2O	0.1584
				CO_2	0.3423
				N_2	0.0075

Boundary conditions for the two reactors were derived from a preliminary process simulation. The CLOP reactors are fed with compressed air during the oxidation stage and a mix of syngas from the gas clean-up unit and combustion products from the CLC reactors during the reduction stage. The mix of fuel and combustion products during the reduction stage determines the average reactor temperature, which is an important parameter to control in the CLOP process. Details of these three streams are given in Table 1.

2.3.1. Solver settings

The commercial CFD package, FLUENT 16.1 was used as the flow solver to carry out the simulations. The phase-coupled SIMPLE algorithm [26] was selected for pressure-velocity coupling, while the QUICK scheme [27] was employed for discretization of all remaining equations. 2nd order implicit temporal discretization was used.

3. Integration of CLOP and PBCLC into a complete power plant

Fig. 4 reports the path flow diagram of the power plant simulated in this work. It integrates the previously detailed reactors cluster with a gasification island and a combined cycle power plant.

3.1. The gasification system

The gasification system selected to deliver the coal-derived synthesis gas to the CLOP system and to the power island follows the High-Temperature Winkler (HTW™) concept [28]. The HTW™ gasification process was originally designed to utilize a low-rank feedstock such as coals with high ash content, lignite, biomass, etc. It is basically a bubbling fluidized bed, where coal devolatilization, partial oxidation and gasification of coal char and volatiles take place.

The bubbling fluidized bed gasifier has been selected instead of an entrained bed gasification system [29] usually adopted in IGCC plants because the high solids residence times allow a high carbon conversion with moderate gasification temperature (below 1000 °C). This is a necessary condition for this plant, provided that the O_2/CO_2 gasification agent from the CLOP unit has a low O_2 content and a substantial coal oxidation would result if a high temperature entrained flow gasification technology is applied.

The HTW™ process involves a gasification unit consisting of a feeding system, the gasifier itself, a bottom ash removal system and a syngas exit in the head of the gasifier with a cyclone. In the subsequent

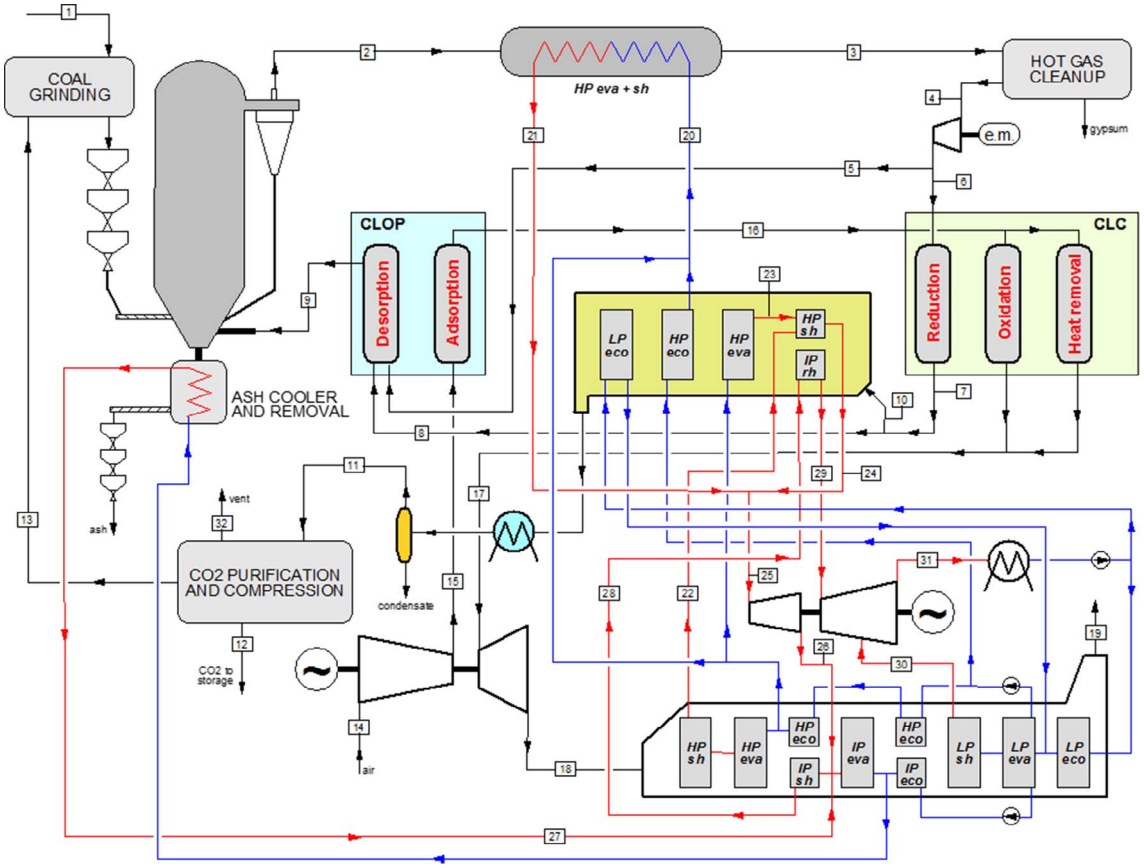

Fig. 4. Schematic of the power plant. Stream flowrates, temperatures, pressures and compositions are indicated in Table 10.

Table 3
Comparison of main results for HTW™ gasifier calibration.

	GS	Ref. [28]
Freeboard zone temperature, °C	900	900
Carbon conversion efficiency, %	95.5	95.5
Syngas composition (N_2 and H_2O free), %		
CO	43.87	45
H_2	35.55	34
CO_2	16.57	17
CH_4	4	4
Specific O_2 consumption, $Nm^3/kg_{coal\ (d.a.f.)}$	0.405	0.39
Cold gas efficiency (HHV basis), %	85.36	85

steps, the raw syngas is cooled, de-dusted and further treated in accordance to the needs of the downstream processes.

Due to the gasifier pressure, a lock-hopper system is used for coal feeding. The coal gasification is controlled by using steam and the O_2/CO_2 oxidizing stream from the CLOP injected into the gasifier via separate nozzles. The nozzles are arranged in several levels located in both the dense zone of the fluidized bed and the freeboard zone (i.e. the post-gasification zone). A high material and energy transfer rate is achieved in the fluidized bed and this ensures a uniform temperature distribution throughout the bed. In order to avoid the formation of particle agglomerations, the temperature is maintained below the ash softening point. Additionally, the gasification agents are injected into the post-gasification zone in order to improve the syngas quality by increasing the temperature and favouring TAR cracking. In summary, the industrial-scale pressurized HTW™ process features two temperature zones, namely the fluidized bed, with an operating window between 800 and 1000 °C, and a post-gasification zone with temperature levels between 900 and 1200 °C [28]. The cyclone separates the entrained solids from the syngas and returns them to the fluidized bed of the gasifier, thus increasing the overall carbon conversion rate.

The performance of the gasifier has been formerly simulated in GS code [30] based on the data reported in open literature [28] in case of gasification of a German lignite with oxygen. An equilibrium calculation at the freeboard zone temperature has been simulated by (i) tuning the required O_2 input flow rate, (ii) fixing the carbon conversion efficiency and (iii) freezing an amount of CH_4 (otherwise not present after equilibrium calculation) to match the data reported by Toporov and Abraham [28]. In addition, steam has been also added to control the CO-to-CO_2 ratio in the final syngas. The equilibrium calculation is validated by the results reported in Table 3, as both the syngas quality, the specific O_2 consumption and the cold gas efficiency (Eq. (16)) are appreciably reproduced.

Table 4
Composition (wt%) and heating values (MJ/kg) of the Douglas Premium Coal considered as feedstock in this work.

C	66.52
H	3.78
O	5.46
N	1.56
S	0.52
Moisture	8
Ash	14.15
HHV	26.23
LHV	25.17

Table 5
Main assumptions for gasification station calculations.

Gasification pressure, bar	15.7
Freeboard temperature, °C	900
Carbon conversion, %	95.5
CO_2 for coal loading, wt% of feedstock	15
Pressure/temperature of CO_2 for coal loading, bar/°C	42/80
Heat loss in syngas cooler, % of transferred heat	0.7
Recycle fan polytropic efficiency, %	85
Recycle fan electric-mechanical efficiency, %	94
Overpressure of the oxidizer from the CLOP system, kPa	50
Electric consumptions for coal milling and handling, kJ_{el}/kg_{coal}	40
Electric consumptions for ash handling, kJ_{el}/kg_{ash}	200
Ash temperature after heat recovery, °C	300

$$CGE = \frac{\dot{m}_{syngas} \cdot HV_{syngas}}{\dot{m}_{feedstock} \cdot HV_{feedstock}} \quad (16)$$

When simulating the new gasification system for the power plant here investigated, a low-sulphur coal has been considered (Table 4), as previously adopted for other power plant performance assessments [9].

In order to reproduce the performance of the HTW™ gasification system with another feedstock, the amount of the oxidizer has been set to achieve the gasifier outlet temperature of 900 °C. In addition, the CH_4 content in the coal-derived gas has been fixed in order to maintain the same value of 11.1% of the ratio between the lower heating value associated to the CH_4 in the syngas and the thermal input related to the feedstock, as achieved in the former calibration simulation.

As anticipated, coal loading is carried out by means of a lock-hopper system with a recycled CO_2 stream from the CO_2 compression station (stream 13 in Fig. 4). The ratio between the recycled CO_2 mass flow rate and the feedstock has been set at 15%. A fraction of 10% of such a CO_2 recycle, is assumed to be vented during normal operation of the lock-hoppers. The main assumptions for gasification station calculations are reported in Table 5. In particular, the gasifier pressure results from the pressure ratio of the gas turbine compressor, with all pressure losses included.

3.2. Hot fuel gas clean-up

The syngas delivered by the gasifier at 900 °C is cooled to 400 °C by HP steam production and superheating. Sulfur species are removed in a hot gas desulfurization unit operating at 400 °C by means of a zinc-based sorbent. The integration of the hot gas desulfurization process in coal gasification-based combined cycles has been thoroughly investigated by the authors in the past [31,32], as a solution to improve the power plant performance. High temperature desulfurization is particularly promising in this application because cooling the very large syngas flow rate exiting the gasifier to nearly ambient temperature would cause major energy penalty and high capital cost compared to conventional cold gas clean-up. On the other hand, a thermodynamic assessment of power plant performance with conventional cold gas clean-up is also included in the result section, in order to better realize the enhancement achievable with hot gas desulfurization.

A schematic of the HGCU (hot gas clean-up) station based on zinc titanate sorbent considered in this work is shown in Fig. 5. The system is based on two interconnected transport reactors where H_2S sorption (Eq. (17)) and sorbent regeneration (Eq. (18)) occur [33].

$$\text{absorption: } ZnO + H_2S \rightarrow ZnS + H_2O \quad (17)$$

$$\text{regeneration: } ZnS + \frac{3}{2}O_2 \rightarrow ZnO + SO_2 \quad (18)$$

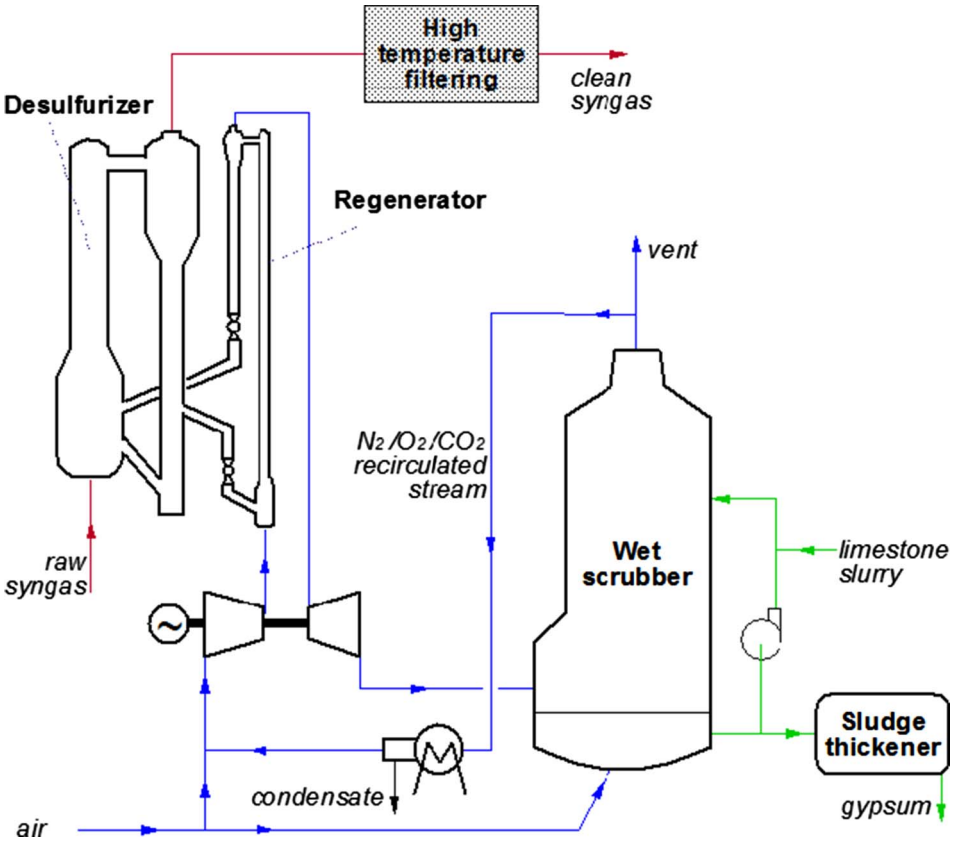

Fig. 5. Schematic of the HGCU station.

Table 6
Main assumptions for HGCU station calculations.

Desulfurization pressure, bar	15.2
Desulfurization temperature, °C	400
Regeneration temperature, °C	750
O_2 molar fraction in the regeneration stream, %	10
ZnS to ZnO molar ratio in the regenerated sorbent	0.1
Compressor/expander polytropic efficiency, %	0.8
Electric-mechanical efficiency, %	0.9
Electric consumption of auxiliaries for the WFGD system, MJ_{el}/kgH_2S	5.34
SO_2 removal efficiency in the WFGD system, %	95
Pressure loss at the hot gas filter, %	5

Table 7
Main assumptions for gas turbine performance calculation.

Air filter pressure loss, %	1
Compressor pressure ratio	17
Compressor polytropic efficiency*, %	92.5
Compressor leakage, % of the inlet flow	0.75
Pressure loss through the CLOP and the CLC system, %	8
Cooled turbine stage isentropic efficiency*, %	91.15
Uncooled turbine stage isentropic efficiency*, %	92.15
Consumption of turbine auxiliaries, % of gross power	0.35
Electric generator efficiency, %	98.7

* Efficiency of large compressor and turbine stages. The actual efficiency is calculated by GS built-in correlations as a function of the actual size of the machine [37].

Hydrogen sulfide is captured in the desulfurization reactor by the circulating sorbent, which is subsequently regenerated in order to be used in several desulfurization cycles. Sorbent regeneration involves the conversion of zinc sulfide into zinc oxide by means of an oxidizing stream. The gas used for sorbent regeneration is O_2 diluted with N_2. O_2 dilution is performed to facilitate heat removal from the regenerator and to reduce the risk of undesired zinc sulfate formation [34,35]. In a conventional IGCC based on oxygen-blown gasification, some nitrogen delivered by the ASU can be used to dilute fresh air and to reduce oxygen concentration in the sorbent regeneration stream [36]. Nevertheless, no ASU is present in the current power plant. Thus, as assumed in other air-blown gasification-based IGCC [32], the N_2-rich gas exiting the regenerator is expanded in a turbine, sent to a wet scrubber for SO_2 absorption and partly recirculated to be used as a diluting agent of the fresh air blown into the regenerator. Details of the calculation assumptions for the HGCU station are reported in Table 6.

The H_2S-free syngas exiting the HT filtering system, i.e. stream 4 in Fig. 4, is boosted by a recycle fan before splitting to the CLOP and the PBCLC systems.

3.3. Heat integration and power island

Three main heat exchange sections are included in the plant layout in Fig. 4.

- A three-level HRSG recovers heat from the exhaust stream exiting the gas turbine. However, considering the TOT of the gas (around 515 °C), steam superheating and reheating are completed outside the HRSG, in the CLC exhaust cooler.
- A HT syngas cooler is present at the exit of the gasifier to cool the syngas down to the desulfurization temperature. Such a syngas

Table 8
Main assumptions for steam cycle calculations.

HRSG gas side pressure loss, kPa	3
HRSG heat loss, % of transferred heat	0.7
HP/MP/LP level, bar	144/36/4
HP/MP/LP turbine isentropic efficiency, %	92/94/88
Maximum live steam temperature, °C	565
Minimum pinch point ΔT, °C	10
Sub-cooling ΔT at drum inlet, °C	5
Minimum stack temperature, °C	80
Pressure losses in economizers, %	25
Pressure loss in super-heaters, %	7
Condensing pressure, bar	0.048
Electric consumption for heat rejection, MJ_{el}/MJ_{th}	0.008
Pumps hydraulic efficiency, %	80
Turbine mechanical efficiency, %	99.6
Electric generator efficiency, %	98.5

Table 9
Main assumptions for CO_2 compression calculations.

LP/HP number of intercooled compression stages	1/3
Compressor stage isentropic efficiency, %	80
Mechanical-electric driver efficiency, %	94
Pressure loss in intercoolers, % of the inlet pressure	2
Intercoolers outlet temperature, °C	30
Liquid CO_2 conditions at pump inlet, bar/°C	80/23
Liquid CO_2 to storage, bar	150
Pump hydraulic efficiency, %	75
Mechanical-electric driver efficiency, %	90
Electric consumption for heat rejection, MJ_{el}/MJ_{th}	0.008

cooler provides heat for HP steam production and superheating up to 565 °C.

- A CLC exhaust cooler is present at the exit of the CLC system for heat recovery from the CO_2-rich stream, used for: (i) HP steam production and superheating, (ii) re-heat of IP steam, (iii) completing the hot temperature superheating of the HP steam from the heat recovery steam generator (HRSG) and (iv) economizing HP and LP water.

A smaller heat exchange unit is also present to cool the solid by-products exiting the bottom of the gasifier down to 300 °C, with IP steam production.

Regarding the turbomachinery in the power plant, a large-size gas turbine is used for the topping cycle, with a pressure ratio of 17 at the compressor and a turbine inlet temperature of 1165 °C, determined by the PBCLC process (stream 17 in Fig. 4). As anticipated for the gasification system, the in-house code GS has been used for the calculation of the plant mass and energy balances. The use of GS is mainly justified by its capability of reliably calculating the cooled expansion of a gas turbine engine. The model [37] is based on a stage-by-stage calculation approach taking into account the blade cooling needs and it has been successfully applied in past works to calculate a variety of IGCC plant configurations [38–40]. The assumptions for gas turbine and steam cycle simulation in Tables 7 and 8 are consistent with the ones adopted in a previous work by the authors [9].

3.4. CO_2 purification and compression

Ultimately, a CO_2 purification and compression station is present to treat the stream exiting the HT exhaust cooler downstream of the PBCLC system. CO_2 purification is necessary to increase the CO_2 content from ~94 vol% (stream 11 in Fig. 4) to a final assumed purity of 97 vol

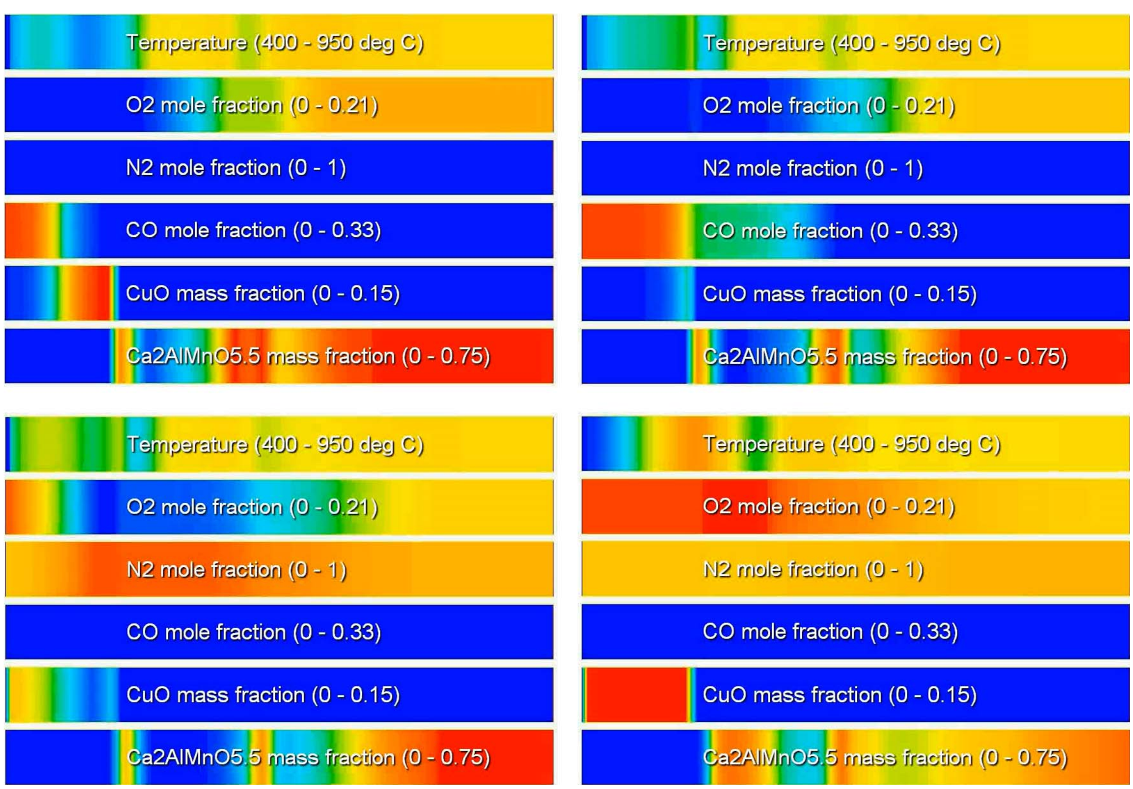

Fig. 6. Four stills from the attached animation, CLOP_animation.mp4, showing contour plots of the CLOP operation (flow from left to right through the domain). The top two images show the middle and end of the reduction stage and the bottom two images show the initial stages and middle of the oxidation stage. Numbers in brackets on each contour plot indicate the range on the blue-green-red colourmap where the low number represents blue and the high number represents red. Note that $Ca_2AlMnO_{5.5}$ is the oxidized state of the CAM material and CuO is the oxidized state of the Cu-based OCM. (For interpretation of the references to colour in this figure legend, the reader is referred to the web version of this article.)

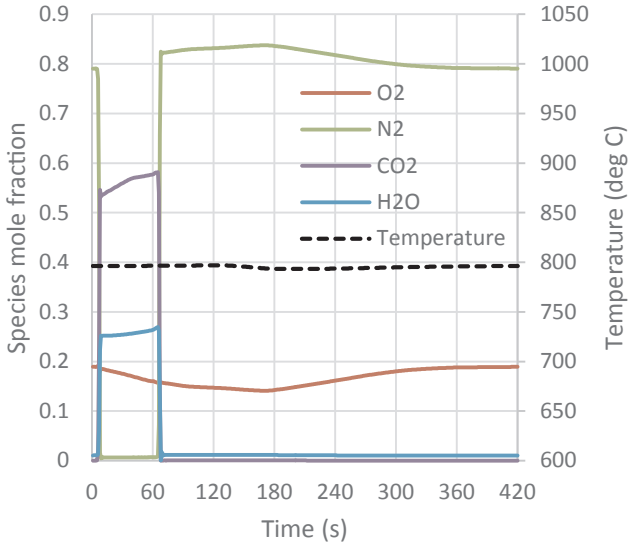

Fig. 7. Transient species and temperature profiles at the outlet of the CLOP reactor illustrated in Fig. 6. The inlet composition is switched to reduction at 0 s and to oxidation at 60 s according to the specifications in Table 1.

%. The CO_2 purification and compression station has been simulated considering a self-refrigerated two-stage separation process based on the same configuration presented in [41].

Cryogenic separation of incondensable gases takes place at 34 bar in two different knockout drums (respectively at −22 °C and −53 °C) where the bulk of CO_2 is condensed in order to remove the incondensable gases remaining in the vapor phase. Some CO_2 is lost in the vapor phase, leading to a CO_2 separation efficiency of 99.1%. About half of the incondensable gases remain in solution in the liquid CO_2 stream, justifying the final purity of 97%. The purified CO_2-rich liquid stream is then vaporized and taken to 80 bar in a three-stage, intercooled compressor. The stream is finally condensed at 23 °C and pumped to the final delivery pressure of 150 bar. Simulation of the CO_2 purification and compression unit has been performed by Aspen Plus™ software. The main assumptions used for the simulation are reported in Table 9.

4. Results and discussion

4.1. Process unit simulations

In this section, results from the CLOP and PBCLC simulations will be presented and discussed for two main purposes: to illustrate the behaviour of these new reactor technologies and to provide modelling guidelines to the subsequent power plant simulations.

4.1.1. CLOP reactor simulations

4.1.1.1. Reactor behaviour. CLOP reactor behaviour is best illustrated by the animation, CLOP_animation.mp4, attached to this submission. Four stills from this animation are presented in Fig. 6 and discussed below.

The top two images of Fig. 6 (reduction stage) clearly illustrate the function of the CLOP reactor: separation of oxygen and nitrogen. Both images show high oxygen concentrations at the reactor outlet, but no nitrogen. The top left image also illustrates the function of the Cu-based oxygen carrier in the initial part of the reactor: combusting the fuel gases. This can be seen from the reaction front of CO reducing CuO. The temperature in the initial part of the reactor is increased by this exothermic reaction. At the end of the reduction stage (top right), some CO slips past the CuO and reacts with the free oxygen released from the CAM material.

Oxygen release from the CAM material can only take place when the local oxygen mole fraction is lower than the equilibrium mole fraction at a given temperature. This reaction therefore takes place in regions of low oxygen mole fractions and high temperatures (the equilibrium oxygen partial pressure increases with temperature according to Eq. (5)). Closer inspection of the top two images in Fig. 6 shows that these conditions are met in the central regions of the reactor, leading to some oxygen release. The end of the reduction stage (top right of Fig. 6) still shows a large region of unconverted $Ca_2AlMnO_{5.5}$ towards the end of the reactor, implying that the reduction stage could have been extended significantly. The discussion on the effect of longer stage times is postponed to Fig. 8.

The initial part of the oxidation stage (bottom left image in Fig. 6) shows the oxidation front moving through the Cu-based material at the start of the bed. This oxidation reaction consumes all the incoming oxygen and all oxygen still visible towards the outlet of the reactor is released by the CAM material. When the Cu-based material is completely oxidized (bottom right image in Fig. 6), the local oxygen mole fraction can exceed the equilibrium mole fraction and the CAM material can once again be oxidized. As the oxidation stage continues and the reactor is heated up by the exothermic oxidation reaction, the equilibrium oxygen mole fraction also increases, implying that only a small fraction of the incoming oxygen can react. This requires a very long oxidation stage, which can be afforded in the COMPOSITE concept because the hot depleted air stream emerging from this stage is directly utilized in the PBCLC reactors (see Fig. 1).

Fig. 7 gives outlet species and temperature profiles for the CLOP reactor. The separation of oxygen from nitrogen during the reduction stage (first 60 s) is clearly visible. It is also clear that the nitrogen concentration at the outlet does not drop immediately at the start of the reduction stage, but shows a ~7 s lag time as it is purged out of the reactor by the incoming sweep gases. Since the reduction stage is only 60 s long in this case, significant mixing of N_2 and CO_2 will occur if the outlet gases are switched at the same time as the inlet gases. For this reason, a 7 s time delay between the inlet switch and the outlet switch is implemented. In this case, the separation between the reduction and oxidation streams is very good due to the plug flow nature of the packed bed reactor. Separation efficiency amounted to 98.9%, implying that 1.1% of the reduction stage outlet gas exits during the oxidation stage and is replaced by gases from the oxidation stage. This will slightly reduce the CO_2 capture efficiency and CO_2 purity from the process.

4.1.1.2. Sensitivity study. The sensitivity of CLOP reactor performance to three important parameters is shown in Fig. 8. CLOP reactor performance is primarily measured by the oxygen concentration achieved in the outlet stream from the reduction stage going to the gasifier (see Fig. 1). A higher oxygen concentration will lead to a smaller gasifier and gas clean-up unit, better gasifier performance, and smaller thermodynamic losses related to the cooling down of the syngas stream before gas clean-up and boosting of the cleaned syngas to overcome the pressure drops in the different process units.

As expected, an optimum reactor operating temperature is clearly visible in Fig. 8 (top). This graph was created by changing the amount of fuel in the reduction inlet gases by changing x in Table 1. High average reactor temperatures favour the oxygen uncoupling reaction, leading to high O_2 concentrations in the reduction outlet gases. If the reactor temperature becomes too high, however, the oxygen carrier cannot be sufficiently oxidized to store the amount of oxygen needed for release in the subsequent reduction stage. In this case, an increase in reactor temperature boosted performance up to an average reactor temperature of 810 °C, after which performance started to decline.

The middle graph in Fig. 8 illustrates a similar optimum with regard to the cycle time. Simulations in this set were performed by changing the reduction and oxidation stage times proportionately. In addition, the amount of Cu-based oxygen carrier at the start of the reactor was increased proportionately with the reduction time (1 m for every 30 s of reduction time) to ensure that the reactor always contains just enough

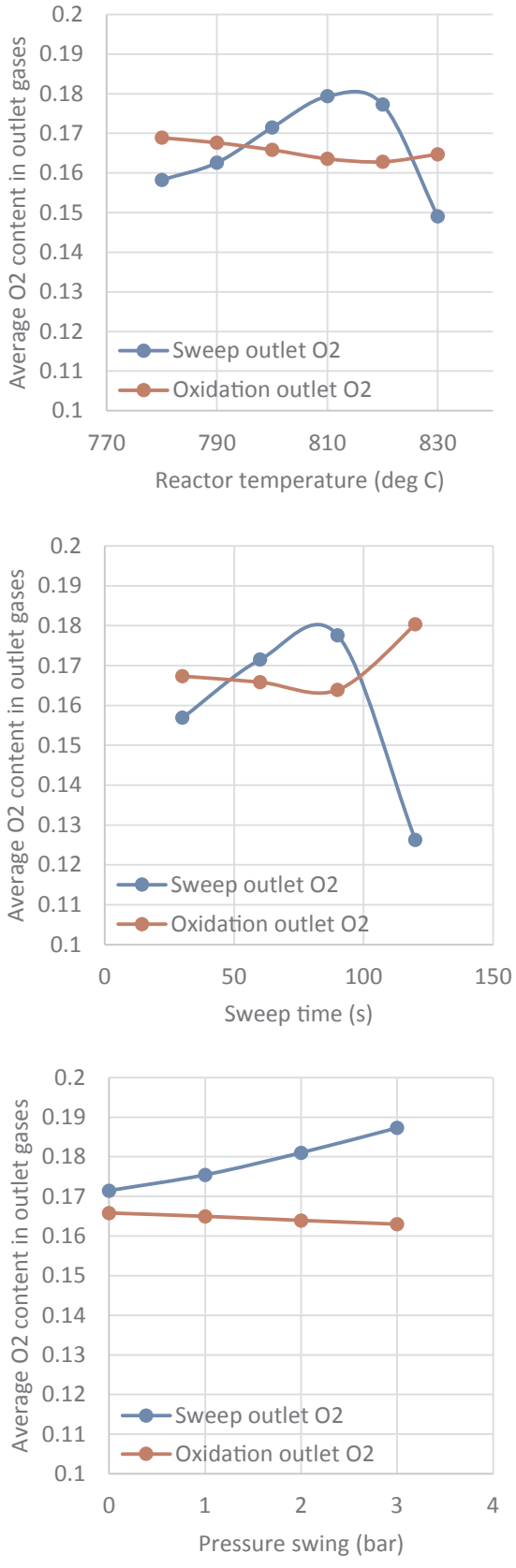

Fig. 8. Sensitivity of the oxygen concentrations in the outlet streams from the reduction and oxidation stages of the CLOP reactor to the average reactor temperature (top), the cycle time (middle) and the degree of pressure swing (bottom).

CuO to convert the fuel entering during the reduction stage. As the cycle time is increased, the deviation from equilibrium at the start of each stage also increases, thus leading to significantly faster kinetics over most of the stage. If the cycle time is increased too much, however, the amount of CAM material becomes insufficient to store the oxygen needed for release during the reduction stage. This is due to the longer oxidation and reduction stage times and the gradual replacement of CAM material with Cu-based oxygen carrier to combust more fuel as the cycle time is increased.

Finally, Fig. 8 (bottom) shows a moderate positive effect of pressure swing on reactor performance. This graph was created by specifying a fixed pressure difference between the outlet pressures of the oxidation and reduction stages, with the reduction stage pressure being the lowest. A lower absolute pressure in the reduction stage causes a higher oxygen mole fraction at a given equilibrium oxygen partial pressure. Even though the advantage brought by pressure swing is significant, this could be difficult to implement in practice. As stated earlier, a delayed outlet valve switch is implemented to minimize contact between N_2 and CO_2. A significant pressure difference between stages would cause operational problems with this strategy and other solutions like a short steam purge between stages would need to be implemented to minimize mixing of N_2 and CO_2.

4.1.1.3. Guidelines for power plant modelling. Following this investigation, the following CLOP reactor modelling guidelines are proposed for the power plant simulations:

- The O_2 mole fraction in the reduction outlet stream going to the gasifier should be set 0.5%-points higher than the O_2 mole fraction in the oxidation outlet stream going to the PBCLC units in the base case. Both better and poorer reactor performance should be investigated given the sensitivity to operating conditions reported in Fig. 8 and the uncertainties related to the CAM material kinetics.
- The outlet gas temperatures from the two stages can be assumed identical.
- A delayed outlet switch can achieve 98.9% separation of the reduction and oxidation outlet gases, but no pressure swing can be implemented in this case.
- The average pressure drops in the reduction and oxidation stages amounted to 0.59 and 0.8 bar respectively.

4.1.2. PBCLC reactor simulations

4.1.2.1. Reactor behaviour. Since there are no equilibrium considerations in the PBCLC system, reactor behaviour is simpler than for the CLOP reactor. The animation, PBCLC_animation.mp4, attached to this submission best illustrates PBCLC reactor dynamics. Four stills from the animation are shown in Fig. 9.

The top left image in Fig. 9 shows the reduction front moving through the bed. It is clear that CO and CH_4 react slowly (wide reaction front), while H_2 reacts faster (narrow reaction front). The slow reaction of CO and CH_4 would cause a lot of undesired fuel slippage had it not been for the hot region from the previous oxidation which remains close to the reactor outlet. As shown in the top right image, the reactions of CO and CH_4 are much faster in this region (narrow reaction fronts), thus preventing fuel from slipping out of the reactor. However, a small amount of unconverted Fe_2O_3 remains in the region before the exiting heat front by the end of the reduction stage. This will slightly reduce the temperature rise in this region in the next oxidation stage.

During the oxidation stage, the reaction front moves through the bed in a similar fashion (bottom left image in Fig. 9). In order to maximise the reactor outlet temperature, while not heating the OCM beyond a temperature of 1200 °C, the oxidation stage needs to be timed correctly so that the reaction front arrives at the reactor outlet just as

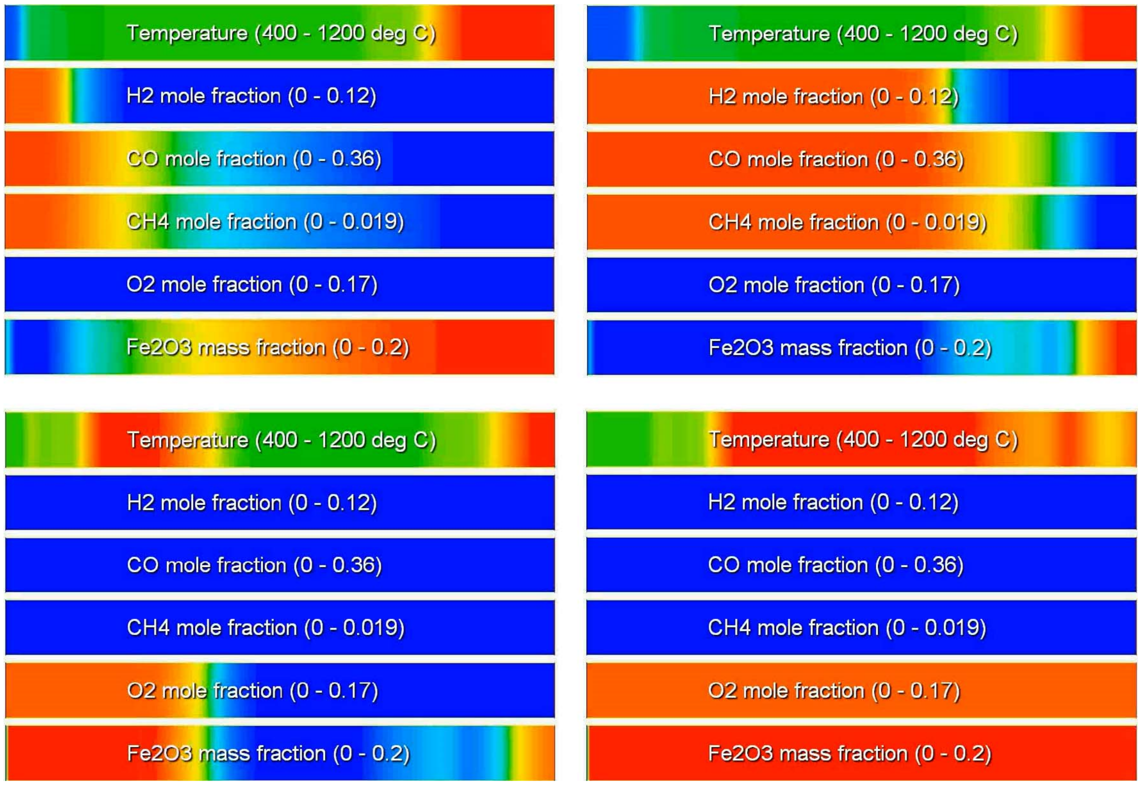

Fig. 9. Four stills from the attached animation, PBCLC_animation.mp4, showing contour plots of the PBCLC operation (flow from left to right through the domain). The top two images show the middle and end of the reduction stage and the bottom two images show the middle and end of the active oxidation stage. Air is still fed for a long time after the active oxidation stage without any reactions taking place in order to remove the heat stored in the reactor. Numbers in brackets on each contour plot indicate the range on the blue-green-red colourmap where the low number represents blue and the high number represents red. Note that Fe_2O_3 is the oxidized state of the ilmenite OCM. (For interpretation of the references to colour in this figure legend, the reader is referred to the web version of this article.)

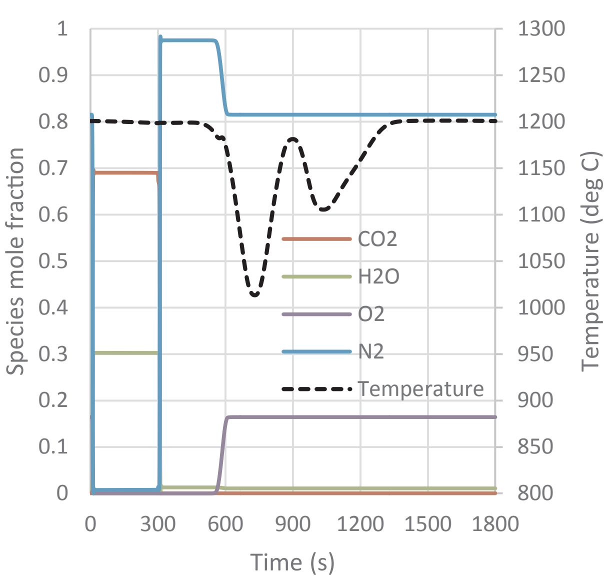

Fig. 10. Transient species and temperature profiles at the outlet of the PBCLC reactor illustrated in Fig. 9. The inlet composition is switched to reduction at 0 s and to oxidation at 300 s according to the specifications in Table 2.

the heat created by the previous oxidation stage exits.

Outlet profiles of species mole fractions and temperature are shown in Fig. 10. The temperature profile shows two distinct dips in the outlet temperature. These two regions of slightly lower temperature can also be seen towards the reactor outlet in the bottom right image in Fig. 9. The first dip is due to the diffuse nature of the heat and reaction fronts, which does not allow for perfect blending between the arriving reaction front and the exiting heat front without overheating the OCM. The second dip is due to the small amount of unconverted Fe_2O_3 remaining before the exiting heat front (bottom left image in Fig. 9).

Fig. 10 also shows excellent separation between CO_2 and N_2. In this case, however, no delayed outlet switch will be implemented to further improve the CO_2/N_2 separation. The cycles are significantly longer than in the CLOP reactor, implying that the impact of a delayed outlet switch will not be so large. For this PBCLC case, the separation efficiency between the reduction and oxidation outlet gases amounted to 97%. This means that 3% of the CO_2-rich reduction stage outlet gases end up in the oxidation stage outlet stream and is replaced by the N_2-rich gases from the oxidation stage, thus reducing the CO_2 capture efficiency and CO_2 purity from the process.

4.1.2.2. Sensitivity study. As mentioned in the previous section, it is important that the oxidation reaction front arrives at the reactor outlet just as the last heat from the previous oxidation stage is exiting. This will achieve the high reactor outlet temperature required for high gas turbine efficiency without exceeding the maximum operating temperature of the OCM. The speed of the heat front moving through the reactor can be controlled by changing the air feed rate. If the air feed rate is too low, the heat front will not exit before the oxidation reaction front arrives, leading to overheating of the OCM. Excessively high air feed rates, on the other hand, will lower the average temperature of the stream sent to the gas turbine.

Fig. 11 shows the effect of the air feed rate on reactor temperatures. An air feed rate of 4.6 kg/m^{2}s appears to be the lowest achievable rate

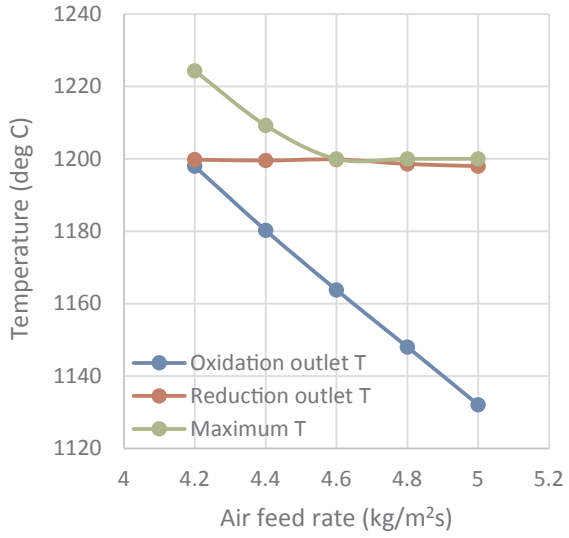

Fig. 11. The effect of air feed rate on the average reactor outlet temperatures and the maximum reactor temperature.

before overheating of the OCM takes place. The resulting temperature of the gas being sent to the gas turbine is 1165 °C, which is significantly below the maximum temperature of 1200 °C. It is possible, however, that the achievement of the maximum reactor outlet temperature at an air feed rate of 4.2 kg/m^2 s will not affect reactor performance because only a small region towards the end of the reactor is overheated by only 25 °C. Raising the gas turbine inlet temperature from 1165 to 1200 °C would increase plant efficiency by ~0.45%-points.

4.1.2.3. Guidelines for power plant modelling. Following this investigation, the following PBCLC reactor modelling guidelines are proposed for the power plant simulations:

- The reactor outlet temperatures are 1165 °C during the oxidation stage and 1200 °C during the reduction stage.
- Complete fuel conversion is achieved.
- A separation efficiency of 97% is achieved between the gases in the oxidation and reduction stages.
- The average pressure drops in the oxidation and reduction stages amounted to 0.77 and 0.27 bar respectively.

4.2. Power plant simulations

The first power plant simulation results detailed in Table 10 refer to the thermodynamic properties of the streams reported in Fig. 4. In particular, they refer to the base case for the next analysis, with high-temperature syngas desulfurization (at 400 °C) and a difference of 0.5 vol% in the O_2 content of the streams exiting the CLOP system at 800 °C. The results in Table 10 have been calculated after setting the coal input at 33.93 kg/s, which is the same input of the power plant previously investigated by the authors dealing with the integration of coal gasification and PBCLC for high efficiency and near-zero emission power generation [9]. The data in Table 10 gives an idea of the size of the components, with particular reference to turbomachinery as well as heat exchanger. Power details for this case, along with overall power plant performance, are detailed in Table 11.

The following sub-sections present results from three sensitivity analyses on the effects of the desulfurization temperature, of the difference in the O_2 content for the two streams exiting the CLOP system and of the temperature at the outlet of the CLOP system.

4.2.1. Effects of syngas cleaning temperature

As described in Section 3.2, hot gas desulfurization is carried out before boosting and splitting the syngas to the CLOP and PBCLC systems. In comparison to the conventional wet desulfurization technology, hot gas clean-up has the advantage of effectively removing H_2S and other sulfide compounds without sensible heat loss and requirement for wastewater treatment. However, hot gas clean-up is not a commercially ready technology [33], so the results of a case with conventional cold gas clean-up (CGCU) are reported as well, in order to allow for accurate benchmarking.

The main results of the power plant simulations, in terms of power balances, are detailed in Table 11. Three cases are reported: the first is characteristic of CGCU, whereas the other two refer to cases with HGCU. Details of the acid gas removal plant layout can be found in a recent work of the authors [40]. Based on the experience gained with these plants, results in Table 11 are calculated according to a heat duty for H_2S stripping of 50 MJ/kg$_{H2S}$ and to an electric energy consumption of 3 MJ/kg$_{H2S}$ for the acid gas removal auxiliaries. After CGCU, syngas is preheated against raw syngas to 300 °C before feeding the CLOP and PBCLC reactors. The two limit values of the desulfurization temperature in the HGCU system have been set based on previous authors' investigations [31,36]. All the cases in Table 11 present a difference of 0.5 vol% in the O_2 content of the streams exiting the CLOP system to the gasifier (oxidizer) and to the PBCLC reactors (depleted air). The temperature of both these streams is set at 800 °C.

Referring to the two cases with HGCU, higher desulfurization temperature does not involve a significantly higher efficiency. Very slight improvements in IGCC efficiency (< 0.1% points) are calculated when raising the desulfurization temperature from 400 to 650 °C. This is mainly due to the relatively small difference of the marginal efficiencies of the topping gas cycle and of the bottoming steam cycle. By increasing the desulfurization temperature from 400 °C to 650 °C, the heat exchanged in the syngas cooler decreases from 119.9 MW (14% of coal input) to 61.7 MW (7.2% of the coal LHV input). As can be appreciated from Table 11, this involves a shift of the power output from the steam turbine, which reduces by 17.9 MW, to the gas turbine, which increases by 20.3 MW. This shift of power output corresponds to a net power output increase of 2.4 MW (0.28% of the coal input). Such a small effect is due to the lower efficiency of the gas cycle compared to a state-of-the-art gas turbine cycles, caused by the lower TIT (< 1165 °C vs. more than 1350 °C) and by the higher pressure drops between the compressor outlet and the turbine inlet (about 9% vs. 4%). On the other hand, the heat used to generate additional high-pressure steam is converted into work at relatively high efficiency, as such steam is superheated and reheated in the HRSG and this leads to a decrease of the irreversibilities related to heat transfer temperature difference between the hot gases and the steam cycle working fluid inside the HRSG. Therefore, providing heat to the gas turbine cycle instead of the steam cycle to evaporate and superheat high pressure steam, makes a small difference from the efficiency standpoint. The slight improvement of the gross efficiency is largely compensated by the higher electric consumption of the syngas recycle blower, which demands more power because of the higher temperature of the syngas at its inlet.

Based on these outcomes, it can be concluded that the desulfurization temperature for the HGCU process should be mainly selected based on technical issues and plant cost considerations rather than on the overall efficiency. A temperature of 400 °C is considered in the cases assessed in the next sections as the reference desulfurization temperature, according to the poorer improvement possible in case of HGCU at 650 °C and to the technological issues related to the higher operating temperature of the syngas recycle blower.

If cold and hot gas clean-up options are compared, it can be seen from Table 11 that HGCU process brings about 2%-points of net electric efficiency improvement. The worse performance of the CGCU case is mainly due to the large amount of low temperature heat rejected to the ambient, which leads to a reduction of the gross efficiency of 2.3% points. It has also to be noted that the syngas recycle blower demands almost the same power in the CGCU and HGCU cases. Although the

Table 10
Thermodynamic properties of the streams reported in Fig. 4.

stream	T, °C	p, bar	$\dot{m}$, kg/s	$\dot{M}$, kmol/s	$\dot{H}$, MW	Ar	CH_4	CO	CO_2	H_2	H_2O	H_2S	N_2	O_2
1	15		33.93	2.134	853.89	Coal composition as in Table 4								
2	900	15.70	166.06	5.591	745.11		2.11	32.51	38.15	9.86	16.03	0.10	1.25	
3	390.6	15.23	166.06	5.591	745.11		2.11	32.51	38.15	9.86	16.03	0.10	1.25	
4	400	14.47	165.97	5.591	742.22		2.11	32.51	38.15	9.86	16.13		1.25	
5	428.1	17.06	77.91	2.625	348.42		2.11	32.51	38.15	9.86	16.13		1.25	
6	428.1	17.06	88.06	2.966	393.79		2.11	32.51	38.15	9.86	16.13		1.25	
7	1200	16.79	111.18	3.080					67.99		28.08		3.40	0.53
8	1200	16.79	14.012	0.388					67.99		28.08		3.40	0.53
9	800	16.20	133.37	3.752					57.93		24.04		1.23	16.81
10	1200	16.79	97.16	2.691					67.99		28.08		3.40	0.53
11	35	15.80	83.67	1.943					94.19		0.36		4.72	0.74
12	38.7	150.0	76.37	1.754					96.97				2.51	0.52
13	80	42	5.09	0.117					96.97				2.51	0.52
14	15	1.01	758.91	26.304		0.92			0.03		1.03		77.28	20.73
15	404.4	17	706.4	24.484		0.92			0.03		1.03		77.28	20.73
16	800	16.20	664.95	23.189		0.97			0.03		1.09		81.60	16.31
17	1165	15.43	641.84	22.448		1.00			0.32		1.27		83.99	13.41
18	508.9	1.06	694.34	24.267		1.00			0.30		1.25		83.49	13.96
19	84.5	1.01	694.75	24.278		1.00			0.30		1.25		83.49	13.96
20	334.9	144	61.12	3.392							100			
21	565	133.92	61.12	3.392							100			
22	483.9	144	33.62	1.866							100			
23	334.9	144	39.36	2.185							100			
24	565	133.92	72.98	4.051							100			
25	565	133.92	134.10	7.443							100			
26	360.73	36	134.10	7.443							100			
27	245	36	2.45	0.136							100			
28	483.9	36	155.71	8.643							100			
29	565	33.48	155.71	8.643							100			
30	300	3.72	8.27	0.459							100			
31	32.17	0.05	163.98	9.102							100			
32	28	1.01	2.14	0.068					23.42		3.65		66.11	6.78

fluid temperature at the compressor inlet is significantly lower in case of CGCU, greater pressure losses are imposed to account for the greater number of heat exchangers [40].

4.2.2. Effects of O_2 content in the stream to the gasifier

Since the performance of the novel CLOP reactor is uncertain at its present state of development, it is important to determine the sensitivity of the COMPOSITE power plant to the difference in the O_2 content (vol%) of the streams exiting the CLOP system. Results showed a low sensitivity of power plant performance to this parameter, thus increasing confidence that the COMPOSITE process can deliver very high efficiency power production. Detailed results of the sensitivity analysis are thoroughly reported in Table A1 (Appendix), for the sake of completeness.

Considering that the amount of oxygen necessary for gasification is related to the (fixed) coal input, a lower O_2 content (vol.%) in the oxidizer brings about a larger mass flow rate of the oxidizing stream (Fig. 12). The resulting syngas is richer in CO_2, has lower heating value and a larger mass flow rate. As a consequence, the heat duty of the syngas cooler increases from 12.8% to 15.6% of the coal heat input when the difference in O_2 content reduces from 2.5 to -1.5% and O_2 concentration in the gasifier oxidant reduces from 18.8 to 14.8%. This variation causes a change of the power share of the gas and steam turbines, but no significant variation is observed in the gross efficiency. The increase of the syngas flow rate also causes an increase of the consumption of the syngas recycle blower. Other items remain unchanged or are subject to slight variations. Focusing on the net LHV efficiency as the main figure of merit, the higher the difference in the O_2 content, the better the performance of the power plant, even if the improvement is really modest (about 0.1% points in the assessed range). It should also be noted that the reduction in syngas flow rate results in smaller size components of the gasification island.

Table 11
Main results of power plant simulations in case of different syngas desulfurization temperature (difference of 0.5 vol% in the O_2 content of the streams exiting the CLOP system at 800 °C).

desulphurization temperature, °C	35	400	650
gas turbine, MW	171.76	177.91	198.21
gas turbine auxiliaries, MW	−0.6	−0.62	−0.69
steam turbine, MW	227.99	241.4	223.47
steam cycle pumps, MW	−3.18	−3.23	−2.83
auxiliaries for steam cycle, MW	−2.73	−2.94	−2.84
HGCU compressor, MW	–	−1.29	−1.29
HGCU expander, MW	–	0.99	0.99
auxiliaries for H_2S removal, MW	−0.56	−1.84	−1.84
syngas recycle blower, MW	−6.18	−6.59	−8.88
CO_2 compression, MW	−12.22	−12.44	−12.45
auxiliaries for heat rejection in the CO_2 compression unit, MW	−0.24	−0.25	−0.25
coal milling and handling, MW	−1.36	−1.36	−1.36
ash handling, MW	−1.16	−1.16	−1.16
balance of plant, MW	−1.28	−1.28	−1.28
Heat input, MW_{LHV}	853.9	853.9	853.9
cold gas efficiency (LHV basis), %	87	86.9	87
gross electric power, MW	399.74	419.31	421.68
net power, MW	370.2	387.3	387.81
gross LHV efficiency, %	46.81	49.11	49.38
net LHV efficiency, %	43.36	45.36	45.42
CO_2 capture efficiency, %	93.1	94.9	95
emissions, $kgCO_2/MWh$	52.87	37.29	36.59
air flow rate at compressor inlet (stream 14), kg/s	736.1	758.9	832.4
air flow rate at turbine inlet (stream 17), kg/s	620.9	641.8	710.6
O_2 in oxidizer (stream 9), %	16.67	16.81	17.19
oxidizer to gasifier (stream 9), kg/s	152.6	133.4	130.2
syngas LHV after cleaning (stream 4), MJ/kg	4.26	4.47	4.56
O_2 in depleted air (stream 16), %	16.17	16.31	16.69

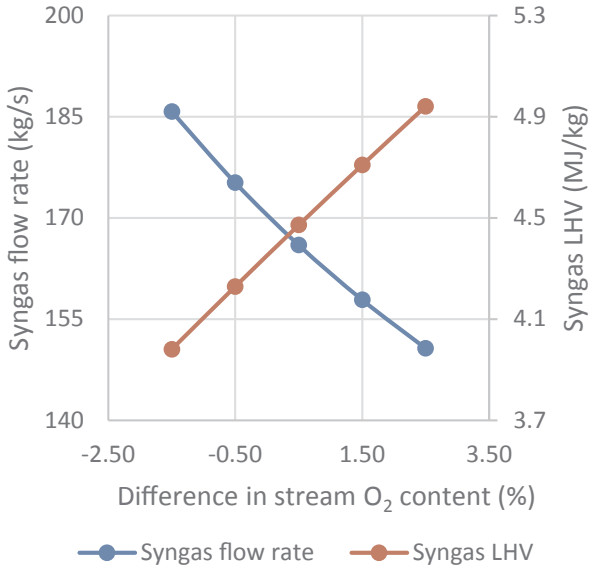

Fig. 12. The effect of the difference in the O2 content (vol.%) of the streams exiting the CLOP system on syngas flow rate and LHV.

4.2.3. CLOP reactor temperature

The most suitable CLOP reactor temperature (i.e. the operating point achieving the optimal equilibrium oxygen mole fraction – Eq. (5)) will be determined by the OCM employed and the system pressure. It will therefore be possible to operate the CLOP system over a range of different temperatures as more OCMs with oxygen uncoupling characteristics become available. For this reason, it is important to determine the sensitivity of the COMPOSITE power plant performance to the operating temperature of the CLOP reactors.

Starting from the base case at 800 °C, lower and higher temperatures have been considered, even though levels higher than 841 °C are not possible in case of a difference of 0.5 vol% in the O_2 content of the streams exiting the CLOP system. This limitation is caused by the low heating value of the syngas, limiting the amount of fuel that can be fed to heat up the CLOP reactor while achieving a given O_2 mole fraction in the outlet gases and a fixed temperature (1165 °C) of stream 17 entering the gas turbine. It is therefore important to note that higher CLOP operating temperatures require better CLOP reactor performance (larger difference between the O_2 content in the streams to the gasifier and the PBCLC reactors) to satisfy the system energy balance.

The results of this sensitivity analysis are thoroughly reported in Table A2. In detail, the lower the CLOP reactor temperature, the higher the amount of oxygen required for coal gasification (less sensible heat is available), but the coal-derived syngas stream is almost the same, with negligible variations of the gas and steam turbine power share and of the electric demand of the recycle blower.

With regard to the other power details, it is possible to appreciate an increasing duty for CO_2 compression, consistent with the CO_2 capture efficiency. CO_2 capture reduces with CLOP reactor temperature because more syngas is directed to the CLC system, where CO_2 slip occurs. Better electric efficiency is obtained in case of lower temperature at the outlet of the CLOP system, even though improvements are again very small (about 0.1% points in the assessed range).

4.3. Benchmarking

Here the COMPOSITE concept is benchmarked against previous authors' studies of PBCLC integrated into coal gasification-based combined cycles [9]. Table 12 concisely reports power details and overall performance of the power plant with integration of coal gasification and packed bed CLC for high efficiency and near-zero emission power generation formerly investigated by the authors [9]. The two cases thoroughly detailed in Table 11 based on CGCU and HGCU at 400 °C are reported as well for a quicker comparison. The same coal input has been used in the current power plant assessment, for consistent comparisons.

On the whole, the gross electric power output of the PBCLC plant is in line with those of the COMPOSITE plants. The main difference among the performance of the two plants is due to the air separation unit, whose power demand amounts to 4% of the fuel energy input (LHV). According to the last consideration, the current power plant based on the COMPOSITE concept is clearly more attractive compared to solutions of PBCLC technology integrated into IGCC systems in terms of electric efficiency.

Compared with the benchmark IGCCs, the COMPOSITE plant with HGCU shows an electric efficiency comparable with the IGCC without capture. The efficiency gain obtained thanks to the lack of the ASU and to the HGCU process counterbalance the penalties associated to the CO_2 compression and the lower gas cycle efficiency due to the lower turbine inlet temperature. Moreover, the item referring to the other auxiliaries

Table 12
Comparison of the main results of IGCC without and with CO_2 capture based on state-of-the-art technologies and of the best power plant layout with PBCLC integrated into coal gasification-based combined cycles [9] vs. the cases with CGCU and HGCU at 400 °C in Table 11.

	IGCC w/o CO_2 capture	IGCC with CO_2 capture	IGCC-PBCLC	COMPOSITE CGCU	COMPOSITE HGCU
gas turbine cycle, MW	227.5*	234.1*	175.1**	171.2	177.3
steam turbine, MW	179.5	161.2	239.8	228	241.4
pumps, MW	−2.9	−3.6	−4.9	−3.2	−3.2
air separation unit, MW	−29.6	−32.7	−33.9		
CO_2 compression, MW		−19.7	−11	−12.2	−12.4
other auxiliaries, MW	−7.2	−22	−14.6	−13.5	−15.7
net power, MW	367.4	317.3	350.5	370.2	387.3
Coal LHV input, MW	812.5	898.8	853.9	853.9	853.9
LVH input to CLC, MW			687	399	393.8
LHV input to CLOP, MW				343.9	348.4
cold gas efficiency, %	81.6	73.2	80.7	87	86.9
gross LHV efficiency, %	50.09	43.98	48.59	46.81	49.11
net LHV efficiency, %	45.21	35.31	41.05	43.36	45.36
CO_2 capture efficiency, %		89.7	96.1	93.1	94.9
emissions, kg_{CO2}/MWh	769.8	101.4	33.4	52.9	37.3

* In the IGCC plant [9], the gas turbine cycle includes the N_2 compressor for coal loading and syngas dilution before combustion in the gas turbine combustor, since compressed nitrogen is eventually expanded in the turbine.

** In the IGCC PBCLC plant [9], the gas turbine cycle includes a main nitrogen compressor and an air compressor to deliver compressed air to the CLC plant, which are conceptually part of the same gas cycle.

does not include specific consumptions related to acid gas removal in case of CO_2 capture by Selexol® [9]. Thus, compared with the benchmark IGCC with CO_2 capture by CO_2 absorption, the COMPOSITE plants show a remarkably higher efficiency of +8 to 10%-points.

5. Summary and conclusions

This work presents a promising new power plant configuration that enables high efficiency power production with CO_2 capture from solid fuels. The COMPOSITE concept is based on an IGCC power plant where chemical looping oxygen production (CLOP) reactors replace the air separation unit and packed bed chemical looping combustion (PBCLC) reactors replace the combustor.

The base-case COMPOSITE power plant, which included hot gas clean-up technology that is not yet commercially available, achieved an electric efficiency of 45.36% and a CO_2 capture efficiency of 94.9%. When cold gas clean-up technology was used, the efficiency dropped to 43.36% – still 2.3%-points higher than a PBCLC-IGCC power plant using a cryogenic air separation unit and 8.1%-points higher than an IGCC plant with pre-combustion CO_2 capture.

Aside from hot gas clean-up, the primary reason for the high efficiency of the COMPOSITE concept is avoidance of the energy penalty associated with air separation via the CLOP reactors. This outcome can only be achieved if the large stream of hot depleted air exiting the CLOP reactors can be efficiently utilized for power production. The COMPOSITE process achieves this outcome by sending this depleted air stream through the PBCLC reactors where it is heated to temperatures suitable for power production in a combined cycle. Additional benefits of this configuration include reduced thermochemical stresses on the PBCLC oxygen carrier material and avoidance of the need for a large N_2-recycle stream if a cheap natural ore is used as the oxygen carrier.

The CLOP system is the most novel component in the COMPOSITE process and therefore has the most uncertainty associated with it. For this reason, sensitivity analyses were completed to assess COMPOSITE power plant performance at different outlet oxygen mole fractions and temperatures from the CLOP reactors. Results showed low sensitivity to both parameters, implying that high electric efficiencies and CO_2 capture can be achieved over a range of CLOP reactor performance.

The outstanding efficiency obtained for the COMPOSITE power plant is possible thanks to a high integration of the different unit operations of the power plant, which can cause process control challenges and limited flexibility. However, given the attractive performance of the COMPOSITE concept assessed in this work, further research is recommended, especially on further development of the CLOP reactor technology, economic analysis and the operability of the whole COMPOSITE power plant.

Acknowledgement

This study was performed as part of the COMPOSITE project “Combined fixed bed processes for improved energy efficiency and low penalty for CO_2 capture”, under the CLIMIT programme; the grant application no. 239802 funded by the Research Council of Norway.

Appendix

See Tables A1 and A2

Table A1
Main results of power plants simulations in case of different O_2 content in the stream to the gasifier (implementing HGCU at 400 °C, with the streams exiting the CLOP system at 800 °C).

Difference in O_2 content, %	−1.5	−0.5	0.5	1.5	2.5
gas turbine, MW	173.75	175.96	177.91–0.62	179.59	181.1
gas turbine auxiliaries, MW	−0.61	−0.62	241.4	−0.63	−0.63
steam turbine, MW	245.65	243.39	−3.23	239.65	238.13
steam cycle pumps, MW	−3.32	−3.27	−2.94	−3.19	−3.15
auxiliaries for steam cycle, MW	−2.97	−2.95	−1.29	−2.93	−2.92
HGCU compressor, MW	−1.29	−1.29	0.99	−1.29	−1.29
HGCU expander, MW	0.99	0.99	−1.84	0.99	0.99
auxiliaries for H_2S removal, MW	−1.84	−1.84	−6.59	−1.84	−1.84
syngas recycle blower, MW	−7.23	−6.89	−12.44	−6.33	−6.1
CO_2 compression, MW	−12.39	−12.41	−0.25	−12.46	−12.48
auxiliaries for heat rejection in the CO_2 compression unit, MW	−0.24	−0.25	−1.36	−0.25	−0.25
coal milling and handling, MW	−1.36	−1.36	−1.16	−1.36	−1.36
ash handling, MW	−1.16	−1.16	−1.28	−1.16	−1.16
balance of plant, MW	−1.28	−1.28		−1.28	−1.28
Heat input, MW_{LHV}	853.9	853.9	853.9	853.9	853.9
cold gas efficiency (LHV basis), %	86.6	86.8	86.9	87.1	87.2
gross electric power, MW	419.4	419.35	419.31	419.25	419.23
net power, MW	386.7	387.02	387.3	387.52	387.76
gross LHV efficiency, %	49.12	49.11	49.11	49.1	49.1
net LHV efficiency, %	45.29	45.32	45.36	45.38	45.41
CO_2 capture efficiency, %	94.5	94.7	94.9	95.1	95.2
emissions, $kgCO_2/MWh$	40.4	38.75	37.29	36.08	34.98
air flow rate at compressor inlet (stream 14), kg/s	743.48	751.69	758.9	765.22	770.82
air flow rate at turbine inlet (stream 17), kg/s	627.71	635.22	641.8	647.62	652.75
O_2 in oxidizer (stream 9), %	14.77	15.79	16.81	17.82	18.83
oxidizer to gasifier (stream 9), kg/s	153.16	142.61	133.37	125.27	118.07
syngas LHV after cleaning (stream 4), MJ/kg	3.981	4.229	4.472	4.709	4.941
O_2 in depleted air (stream 16), %	16.27	16.29	16.31	16.32	16.33

Table A2
Main results of power plants simulations in case of different temperatures at the outlet of the CLOP system (implementing HGCU at 400 °C, with a difference of 0.5 vol% in the O_2 content of the streams exiting the CLOP system).

CLOP system outlet temperature, °C	600	700	800	841
gas turbine, MW	179.2	178.53	177.91	177.68
gas turbine auxiliaries, MW	−0.63	−0.62	−0.62	−0.62
steam turbine, MW	240.74	241.09	241.4	241.5
steam cycle pumps, MW	−3.21	−3.22	−3.23	−3.23
auxiliaries for steam cycle, MW	−2.94	−2.94	−2.94	−2.94
HGCU compressor, MW	−1.29	−1.29	−1.29	−1.29
HGCU expander, MW	0.99	0.99	0.99	0.99
auxiliaries for H_2S removal, MW	−1.84	−1.84	−1.84	−1.84
syngas recycle blower, MW	−6.54	−6.57	−6.59	−6.59
CO_2 compression, MW	−12.16	−12.3	−12.44	−12.49
auxiliaries for heat rejection in the CO_2 compression unit, MW	−0.24	−0.24	−0.25	−0.25
coal milling and handling, MW	−1.36	−1.36	−1.36	−1.36
ash handling, MW	−1.16	−1.16	−1.16	−1.16
balance of plant, MW	−1.28	−1.28	−1.28	−1.28
Heat input, MW_{LHV}	853.9	853.9	853.9	853.9
cold gas efficiency (LHV basis), %	82.8	84.8	86.9	87.8
gross electric power, MW	419.94	419.62	419.31	419.18
net power, MW	388.28	387.78	387.3	387.11
gross LHV efficiency, %	49.18	49.14	49.11	49.09
net LHV efficiency, %	45.47	45.41	45.36	45.34
CO_2 capture efficiency, %	92.7	93.8	94.9	95.4
emissions, $kgCO_2/MWh$	53.74	45.35	37.29	34.09
air flow rate at compressor inlet (stream 14), kg/s	759.97	759.41	758.9	758.73
air flow rate at turbine inlet (stream 17), kg/s	644.58	643.16	641.8	641.33
O_2 in oxidizer (stream 9), %	18.42	17.61	16.81	16.48
oxidizer to gasifier (stream 9), kg/s	133.15	133.41	133.37	133.23
syngas LHV after cleaning (stream 4), MJ/kg	4.267	4.364	4.472	4.521
O_2 in depleted air (stream 16), %	17.92	17.11	16.31	15.98

References

[1] Rubin ES, Davison JE, Herzog HJ. The cost of CO2 capture and storage. Int J Greenhouse Gas Control 2015;40:378–400.
[2] Ishida M, Zheng D, Akehata T. Evaluation of a chemical-looping-combustion power-generation system by graphic exergy analysis. Energy 1987;12(2):147–54.
[3] Lyngfelt A, Leckner B. A 1000 MWth boiler for chemical-looping combustion of solid fuels – discussion of design and costs. Appl Energy 2015;157:475–87.
[4] Mancuso L, Cloete S, Chiesa P, Amini S. Economic assessment of packed bed chemical looping combustion and suitable benchmarks. Int J Greenhouse Gas Control 2017;64:223–33.
[5] Lockwood T. Techno-economic analysis of PC versus CFB combustion technology. IEA Clean Coal Centre; 2013.
[6] IEA. Projected costs of generating electricity. International Energy Agency and Nuclear Energy Agency; 2015.
[7] Lyngfelt A. Chemical-looping combustion of solid fuels – status of development. Appl Energy 2014;113:1869–73.
[8] Abad A, et al. Conceptual design of a 100 MWth CLC unit for solid fuel combustion. Appl Energy 2015;157:462–74.
[9] Spallina V, et al. Integration of coal gasification and packed bed CLC for high efficiency and near-zero emission power generation. Int J Greenhouse Gas Control 2014;27:28–41.
[10] Hamers HP, et al. Comparison on process efficiency for CLC of syngas operated in packed bed and fluidized bed reactors. Int J Greenhouse Gas Control 2014;28:65–78.
[11] Spallina V, et al. Investigation of heat management for CLC of syngas in packed bed reactors. Chem Eng J 2013;225:174–91.
[12] Hamers HP, et al. Energy analysis of two stage packed-bed chemical looping combustion configurations for integrated gasification combined cycles. Energy 2015;85:489–502.
[13] Mancuso L, et al. Economic assessment of packed bed chemical looping combustion and suitable benchmarks. Int J Greenhouse Gas Control 2017;64:223–33.
[14] Shah K, Moghtaderi B, Wall T. Selection of suitable oxygen carriers for chemical looping air separation: a thermodynamic approach. Energy Fuels 2012;26(4):2038–45.
[15] Ergun S. Fluid flow through packed columns. Chem Eng Prog 1952;48:89.
[16] Tsotsas E, Martin H. Thermal conductivity of packed beds: a review. Chem Eng Process Process Intensif 1987;22(1):19–37.
[17] Gunn DJ. Transfer of heat or mass to particles in fixed and fluidized beds. Int J Heat Mass Transf 1978;21:467–76.
[18] Motohashi T, et al. Oxygen storage capability of brownmillerite-type $Ca_2AlMnO_{5+\delta}$ and its application to oxygen enrichment. Chem Mater 2013;25(3):372–7.
[19] Levenspiel O. Chemical reaction engineering. 3rd ed. United States: John Wiley & Sons; 1999.
[20] Abad A, et al. Mapping of the range of operational conditions for Cu-, Fe-, and Ni-based oxygen carriers in chemical-looping combustion. Chem Eng Sci 2007;62(1–2):533–49.
[21] Abad A, et al. Kinetics of redox reactions of ilmenite for chemical-looping combustion. Chem Eng Sci 2011;66(4):689–702.
[22] García-Labiano F, et al. Effect of pressure on the behavior of copper-, iron-, and nickel-based oxygen carriers for chemical-looping combustion. Energy Fuels 2005;20(1):26–33.
[23] Yang W, et al. An effective reaction rate model for gas-solid reactions with high intra-particle diffusion resistance. Int J Chem Reactor Eng 2016;14(1):331–42.
[24] Robie R, Hemingway B. Thermodynamic properties of minerals and related substances at 298.15 K and 1 bar pressure and at high temperatures, U.S.D.o.t. Interior, Editor; 1995.
[25] Stull DR, Prophet H. JANAF thermochemical tables, 2nd ed., U.S.N.B.o. Standards, Editor; 1971: Washington D.C.
[26] Patankar S. Numerical Heat Transfer and Fluid Flow. United States: Hemisphere Publishing Corporation; 1980.
[27] Leonard BP, Mokhtari S. ULTRA-SHARP nonoscillatory convection schemes for high-speed steady multidimensional flow. NASA TM 1-2568 (ICOMP-90-12). NASA Lewis Research Center; 1990.
[28] Toporov D, Abraham R. Gasification of low-rank coal in the High-Temperature Winkler (HTW) process. J South Afr Inst Min Metall 2015;115:589–97.
[29] Giuffrida A, Romano MC, Lozza G. Thermodynamic analysis of air-blown gasification for IGCC applications. Appl Energy 2011;88(11):3949–58.
[30] Gecos. GS Software. www.gecos.polimi.it/software/gs.php; 2014.
[31] Giuffrida A, Romano MC. On the effects of syngas clean-up temperature in IGCCs. In: ASME Turbo Expo 2010; 2010: Glasgow, UK.
[32] Giuffrida A, Romano MC, Lozza G. Efficiency enhancement in IGCC power plants with air-blown gasification and hot gas clean-up. Energy 2013;53:221–9.
[33] Denton DL. An update on RTI's warm syngas cleanup demonstration project. In: Gasification technologies conference; 2014: Washington, DC.
[34] Jothimurugesan K, Gangwal SK. Regeneration of zinc titanate H2S sorbents. Ind Eng Chem Res 1998;37(5):1929–33.
[35] Elseviers WF, Verelst H. Transition metal oxides for hot gas desulphurisation. Fuel 1999;78(5):601–12.

[36] Giuffrida A, Romano MC, Lozza GG. Thermodynamic assessment of IGCC power plants with hot fuel gas desulfurization. Appl Energy 2010;87(11):3374–83.
[37] Chiesa P, Macchi E. A thermodynamic analysis of different options to break 60% electric efficiency in combined cycle power plants. J Eng Gas Turbines Power 2004;126(4):770–85.
[38] Giuffrida A, et al. Lignite-fired air-blown IGCC systems with pre-combustion CO2 capture. Int J Energy Res 2016;40(6):831–45.
[39] Bonalumi D, Giuffrida A. Investigations of an air-blown integrated gasification combined cycle fired with high-sulphur coal with post-combustion carbon capture by aqueous ammonia. Energy 2016;117:439–49.
[40] Moioli S, et al. Assessment of MDEA absorption process for sequential H2S removal and CO2 capture in air-blown IGCC plants. Appl Energy 2016;83:1452–70.
[41] Campanari S, et al. Predicting the ultimate potential of natural gas SOFC power cycles with CO_2 capture – Part B: applications. J Power Sources 2016;325:194–208.